7-21-2017

Nanoscale tilt measurement using a cyclic interferometer with phase stepping and multiple reflections

Tahereh Naderishahab
Rose-Hulman Institute of Technology, naderit@rose-hulman.edu

Nanoscale tilt measurement using a cyclic interferometer with phase stepping and multiple reflections

A Thesis

Submitted to the Faculty

of

Rose-Hulman Institute of Technology

by

Tahereh Naderishahab

In Partial Fulfillment of the Requirements for the Degree

of

Master of Science in Optical Engineering

July 2017

ROSE-HULMAN INSTITUTE OF TECHNOLOGY

Final Examination Report

Tahereh Naderishahab — Name

Optical Engineering — Graduate Major

Thesis Title: Nano Scale Tilt Measurement using a Cyclic Interferometer with Phase Stepping and Multiple Reflections

DATE OF EXAM: July 21, 2017

EXAMINATION COMMITTEE:

	Thesis Advisory Committee	Department
Thesis Advisor:	Charles Joenathan	PHOE
	Robert Bunch	PHOE
	Ashley Bernal	ME

PASSED X **FAILED** _____

ABSTRACT

Naderishahab, Tahereh

M.S.O.E

July 2017

High accuracy tilt or roll angle measurement is required for a variety of engineering and scientific applications. Optical interferometry is normally used because it is non-contact and can measure tilt with a very high degree of accuracy. In this thesis, a cyclic interferometer has been developed with four mirrors to measure tilt angles as small as a few nanoradians. To measure the phase, a novel and simple method of phase shift by polarization was developed to enhance measurement sensitivity and accuracy. Since the cyclic interferometer is insensitive to external vibrations and turbulences, polarization phase step was accomplished with relative ease.

To introduce the phase shift, a quarter wave plate and a half wave plate were used with a polarized laser beam. Multiple reflections were also introduced in the cyclic interferometer to enhance tilt measurement capability. A new method was developed to evaluate phase and eventually measure the tilt even in the case of changing fringe visibility. The results of these studies show that the multiple reflection cyclic interferometer can be used to measure object tilts in the order of 0.2 nanoradians or 10^{-5} arc second.

Dedication

This thesis is dedicated to Mom and Dad and Marzieh, who have always been there for me, supporting me with their love and kindness, picking me up on time, and encouraging me to go on every adventure, especially this one.

Acknowledgment

Dr. Charles Joenathan, thank you for accepting me as your student even when I had only six months left at Rose-Hulman, for guiding me through my studies and for your support and patience.

Dr. Ashley Bernal, thank you for serving on my advisory committee, your kind help with my research, and your guidance in the process of applying to graduate school.

Dr. Robert Bunch, thank you for serving on my advisory committee, for your corrections to my thesis, and for your advice during my time at Rose.

Dr. Craig Downing, thank you for reviewing my thesis and your kind suggestions.

Mr. Roger Sladek, thank you for all of the machining work you have done for my thesis and for your technical advice.

Azadeh Aghighi and Sue Kashanipour, thank you for your precious friendship, your endless support and thank you for being my family while I was away from my parents.

Sanaz Faryadras, thank you for your friendship and kind support.

Deepak Charles, thank you for making my time at school more fun.

Tony Meyer, thank you for your love and support. I would not have finished without you.

I would like to give special thanks to my parents and sister for a lifetime of unconditional love. Thank you for everything.

Table of Contents

LIST OF FIGURES

LIST OF TABLES

1 Introduction

High accuracy tilt measurements on the scale of thousands of arc seconds or nanoradians are often used in different fields of science and engineering including metrology for precision autocollimation and planarity measurements. The measurement of tilt has diverse applications, for example, to control the straightness of the translation stages of x-ray interferometers [1], to control the angle between mirrors in interferometric telescopes used for astrometry [2], to measure the gravitational constant or the Casimir force [3], to measure the cantilever deflection in atomic force microscopes [4] and to measure angular accelerations [5]. Although tilt measurement is a mechanical problem, optical methods are often used.

Interferometry is a highly sensitive tilt measurement optical technique that uses the principle of the interference of two beams generated from the same laser that travels slightly different optical path lengths whenever an angular displacement occurs. The Michelson interferometer is the commonly used device for measuring tilt with high accuracy and sensitivity [6]. A Fabry-Perot etalon along with scanning has also been used to measure tilt with high accuracy [7]. Another interferometric method is the Murty Shear Plate which measures tilt by determining the slope of the wavefront after passing through the shear plate [8]. In addition, heterodyne techniques in interferometry have been used to enable measurements of small tilts in systems [9].

Most recently, a new method using a cyclic lateral shear interferometer has been used in order to measure small tilt angles. In this setup, when the interferometer is rotated, a phase difference is introduced between the two laterally sheared beams, which are then used to measure the rotation [10]. Angles as small as 22 arc secs have been measured. On the other hand, multiple

reflections have been used in metrology to increase the sensitivity of Michelson Interferometers for measuring small linear displacements [11]. The concept of multiple reflections was incorporated in a cyclic interferometer to improve upon the sensitivity to tilt measurement. The cyclic path interferometer with its counter propagating beams is not sensitive to linear displacement, but has been shown to be sensitive to tilt. In comparison to the Michelson interferometer, the cyclic interferometer is twice as sensitive when measuring tilt. It has been shown that the cyclic path interferometer with multiple reflections can be used to measure tilt angles below 5 μrad [10].

In this thesis, the cyclic interferometer has been improved by introducing a novel method of phase stepping to extract phase information, thus allowing tilt measurements down to the nanoscale. It is worth mentioning that since the two counter propagating beams travel the same distance, the system is less sensitive to vibrations and external turbulence. This added stability allows for an easy method to introduce phase stepping by using the polarization of the laser beam. Since the beams are traveling the same path and in the opposite directions, it is not easy to introduce conventional phase stepping tools. It is shown that by using only two additional components in the cyclic interferometer, phase stepping can be introduced with relative ease. Also developed in this thesis are two phase stepping algorithms, namely the four-phase step method and the phase differentiation method.

1.1 Thesis Organization

In this thesis, different approaches for measuring small angle tilts are reviewed. The present chapter will highlight the framework of the thesis.

In Chapter 2, different tilt measurement techniques are explained. Specific interferometers will be discussed, namely the Michelson interferometer, the Heterodyne interferometer, and the cyclic path interferometer.

In Chapter 3, the theory and setup of a cyclic path interferometer are discussed in detail. Also, the tilt measurement procedure using the cyclic path interferometer with phase stepping and phase measurement is described. Two phase stepping routines are discussed in this chapter, namely the four-phase step method, which is used when the visibility of the fringes is not changing, and a modified phase differentiation method, which is used when the visibility of the fringes change with the introduction of phase step.

In Chapter 4, the experimental setup for measuring small angle tilts using the cyclic path interferometer will be explained in detail. The process that leads to a higher sensitivity in the measurements will also be discussed, along with polarization phase stepping.

Chapter 5 will present a summary of the results and simulations of the tilt measurements achieved using the setup explained in Chapter 4. It will also offer concluding remarks, including directions for further research.

2 Optical Techniques for Tilt Measurement

2.1 Introduction

Both interferometric and non-interferometric techniques can be used to measure angular tilt or rotation. In this thesis, the focus will be on the interferometric techniques as they are robust and can be used to measure small tilt needed in many applications.

2.2 Optical Interferometry Used for Measuring Small Tilt Angles

When two or more waves generated from the same coherent source converge, they will interfere with each other. This interference may be constructive or destructive: They will add wherever a peak of one wave match with the peaks of the other. This superposition is called constructive interference. Wherever a peak of one wave falls on the trough of the other wave, they will cancel each other out (or partially cancel, if the amplitudes are not the equal). This is called destructive interference.

If the interference involves two identical waves, with the same amplitude and wavelength, then the waves will have a constructive interference at a certain point if their path lengths up to that point are the same or differ by an integral number of wavelengths. For the waves to interfere

destructively, their path lengths must differ by an integral number of wavelengths plus a half a wavelength [12].

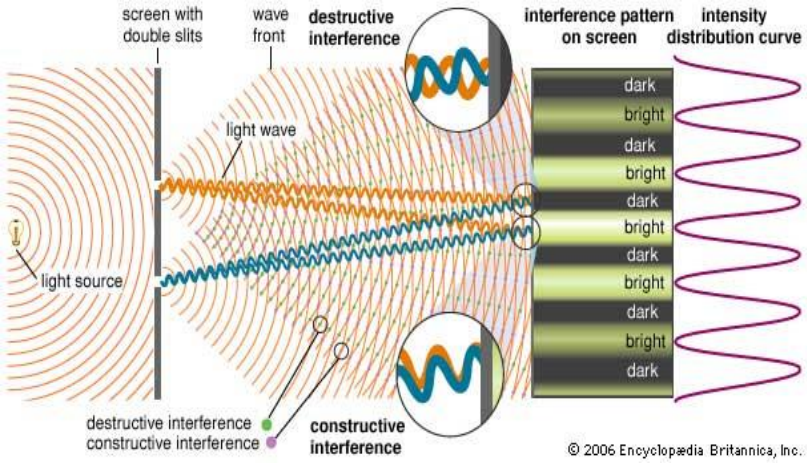

Figure 2.1 An Example of Optical interference, The Young double-slit experiment [12].

Optical Interferometry has been used for examining the quality of optical elements like mirrors, lenses, etc. It looks for and measures any deformation in the optical element's surface. To evaluate these optical elements, highly accurate measurements in the interferometric process are needed. There are several interferometers used for measuring small-angle tilts in systems including the Michelson, heterodyne, and cyclic path interferometers [13, 9, 10]. Also, there are a few techniques that are based on interferometric processes. One such method uses a Murty shear plate [8], while another uses the Fabry-Perot etalon to measure the small-angle tilts in the system [7]. These methods will be explained in detail in the following subsections.

2.2.1 Tilt Measurement Using Michelson Interferometer

As is shown in Fig 2.2, the Michelson interferometer is a common configuration for optical interferometry and was invented by Albert Abraham Michelson. A beam splitter (BS) is used to split the light into two beams that are orthogonal to each other. These two beams are then reflected back to the BS via two mirrors, where they are then combined to form one beam. The amplitudes

of the two beams will combine based on the principles of interferometry causing constructive or destructive interference as explained before. The interfered beam is directed to a screen or a CCD camera or some other type of detector for making the observation [6].

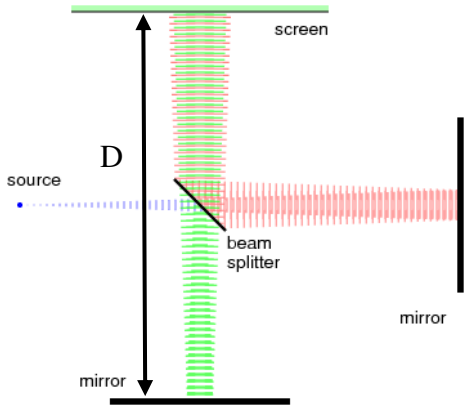

Figure 2.2 Schematic of a Michelson interferometer [14].

Tilt measurements are based on the measurement of the optical path difference (d) between two beams if one of the mirrors is tilted by α in the Michelson interferometer. If D is the distance of the mirror that is tilted to the screen, then:

$$\alpha = d/D \tag{2.1}$$

A disadvantage for this system is its limited resolution. In order to measure small angles, a large distance D is needed between the mirror and the screen or the CCD camera [6].

2.2.2 Tilt Measurement Using Heterodyne Interferometer

The original heterodyne interferometer shown in Fig. 2.3 is used for linear displacement measurements. In this schematic arrangement, two collinear and orthogonally polarized beams with different angular frequencies (ω_1, ω_2) are sent to a Polarizing Beam Splitter (PBS). One of the beams is sent on a fixed retroreflector, while the other is sent on a moving retroreflector. Due

to motion, the beam reflecting from the moving retroreflector will undergo a Doppler shift. Both beams reunite at the back of the PBS, where interference happens. The phase shift of the measurement signal from photo detector 1 is compared to the reference signal from the photo detector 1. The displacement of the moving mirror can then be extracted by measuring the phase shift measured by the two signals [9].

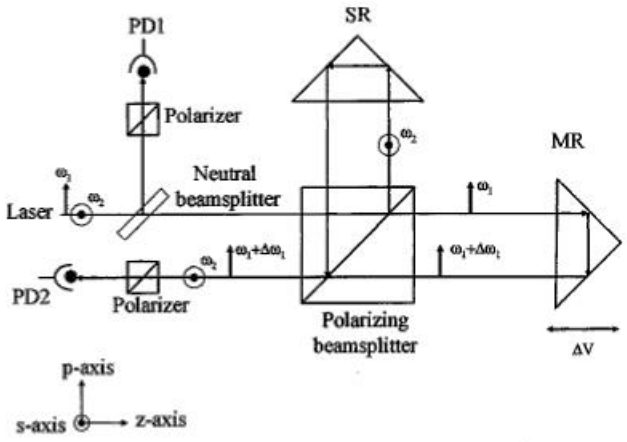

Figure 2.3 Schematic of the Heterodyne interferometer [9].

Chiu et al. introduced a new method for measuring phase from the phase retardation of wave plates using a heterodyne interferometer. Fig. 2.4 shows a linearly polarized light at wavelength of λ_1 or λ_2 passing through an electro-optic modulator. It is incident on a BS and then divided into two equal amplitude beams. The reflected light passes through an analyzer and then enters a photodetector D_r. The transmitted light passes through a tested wave plate as well as an analyzer and is detected by another photodetector D_t. The phase difference between the two beams is then measured using a phase meter [15].

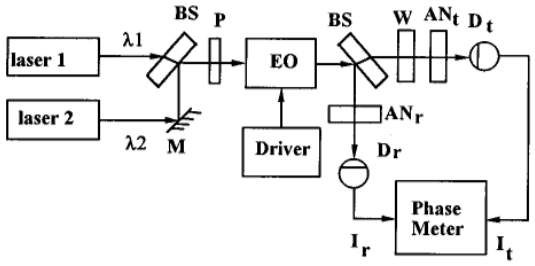

Figure 2.4 Schematic of the heterodyne interferometer proposed by Chiu et al. for measuring phase retardation in wave plates. P, polarizer; BS, beam splitter; M, mirror; EO, electro-optic modulator; AN, analyzer; W, wave plate to be measured; D, photodetector [15].

A modification of the previous setup was later proposed for measuring angles based on the heterodyne interferometer and Total Internal Reflection. The setup shown in Fig. 2.4 is modified by replacing the test waveplate with a movable prism. This modified schematic is shown in Fig. 2.5 [16].

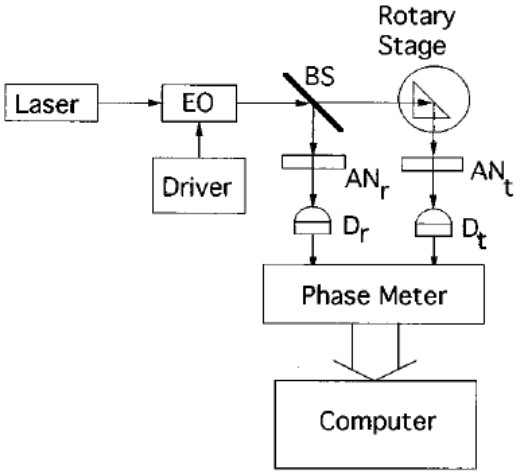

Figure 2.5 Schematic of the setup introduced by Chie and Su for measuring tilt angles. EO: electro-optic modulator; BS: beamsplitter; D: photodetector; AN: analyzer [16].

In this setup, the signal measured by D_t is the test signal, and the signal measured by D_r is the reference signal. The two signals are sent to the phasemeter and their phase difference Φ_r is obtained. Then the test prism is removed so the transmitted light will travel through the analyzer and Dt, this time the phase of the reference signal is measured by the phasemeter to be Φ_t. So, the

phase difference between the s and p polarization is determined due to the total internal reflection and can be expressed as in Eq. (2.2) [9]

$$\Phi = \Phi_t + \Phi_r \tag{2.2}$$

The tilt angle can be calculated by substituting Φ into the Fresnel's Equations. Fresnel's equations describe the reflection and transmission of electromagnetic waves at an interface between two layers with different refractive indices. That is, they give the reflection and transmission coefficients for waves with electric field parallel and perpendicular to the plane of incidence. For light from a medium of index n_1 incident upon a medium of index n_2 at an angle θ_i and the angle of transmission θ_t, Fresnel's equations give the reflection coefficients as follows [9]:

$$r_{\parallel} = \frac{\tan(\theta_i - \theta_t)}{\tan(\theta_i + \theta_t)} \tag{2.3}$$

And

$$r_{\perp} = \frac{sin(\theta_i - \theta_t)}{sin(\theta_i + \theta_t)} \tag{2.4}$$

2.2.3 Tilt Measurement Using Cyclic Path Interferometer

The cyclic path interferometer is a type of two beam amplitude division interferometer which was first discussed by Michelson [17] and Hariharan [18]. The first version of this interferometer was a triangular path cyclic interferometer. This type of interferometer uses a beam splitter to divide the beam into two beams which ideally travel the same loop in opposite directions

before recombining. This type of interferometer offers three main advantages: First, it is very easy to set up. Second, it restricts the degrees of freedom in the system, and third, it decreases the requirements on both the coherence length of the source and the angular stability of the beam. The schematic of the first version of the cyclic path interferometer is shown in Fig. 2.6 [19]. According to Fig. 2.6, the laser beam expansion and collimation is done using the microscope objective and the collimating lens. It is worth mentioning that the light source used in this system was a He-Ne 5 mW laser of 632.8 nm wavelength and was linearly polarized in the TEM_{00} mode.

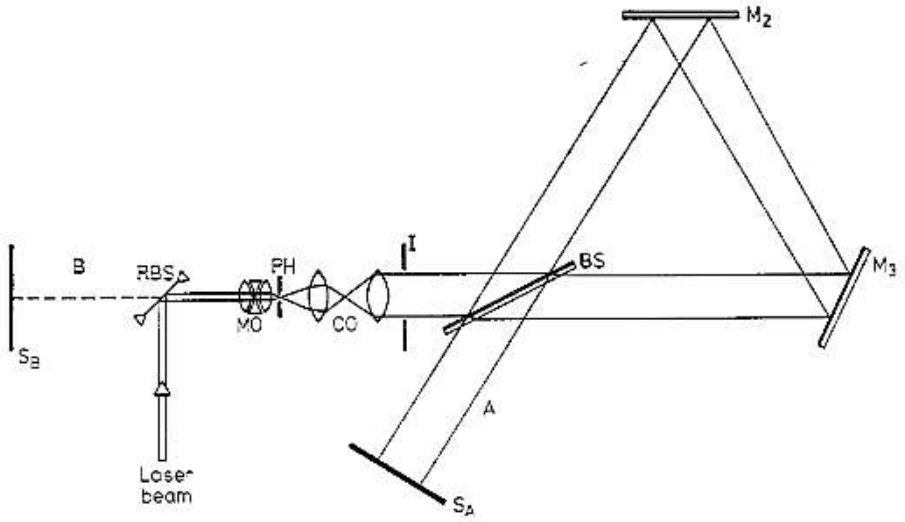

Figure 2.6 Schematic of cyclic interferometer. BS, beam splitter: M. mirror: C, collimator; PH, pinhole; MO, microscope objective; S, screen; RBS, rotational beam splitter; I, iris diaphragm *[19]*.

Kumar et al. presented a new method for measuring small roll angles using the same setup as in Fig. 2.6 [20]. The cyclic interferometer is mounted on a rotary stage, and lateral shear is generated by polarization and which when brought to the same state of polarization by a polarizer produces lateral shear interference fringe. When the cyclic path interferometer is rotated, a phase change is introduced between the orthogonally polarized beams because the incident angle has changed. This results in spatial displacement of the interference fringes. Using polarization phase shifting technique the phase difference between the two beams, is measured [20].

2.2.4 Tilt Measurement Using the Murty Interferometer

The Murty interferometer is a lateral shearing interferometer designed by Murty for testing optical elements [8]. This method, similar to other interferometric methods, is based on the change in the optical path differences between two beams which in this case are the beams reflected from the front and back surfaces of the parallel plate.

This flat parallel plate is shown in Fig. 2.7. The optical path difference between the reflection from

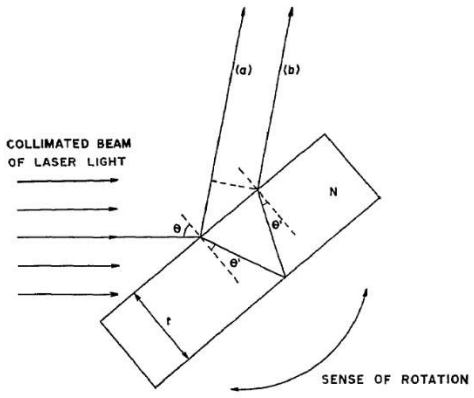

Figure 2.7 Flat-Parallel plate of glass used in Murty interferometer [8].

the back and front surfaces can be expressed as

$$OPD = 2nt\cos\theta' \tag{2.5}$$

Where t is the thickness of the flat plate, n the refractive index of the plate in vacume and θ' is the angle of refraction corresponding to the angle of incidence. In the case of light entering the glass plate at two different angles such as θ_1 and θ_2, the difference between the optical path differences for the rotated and unrotated beam will be

$$OPD_1 - OPD_2 = 2nt(\cos\theta'_1 - \cos\theta'_2) \quad (2.6)$$

According to the Stokes relations, the destructive interference will happen when

$$OPD_1 - OPD_2 = m\lambda \quad (2.7)$$

In which, *m* is an integer and λ is the wavelength of the light source used. Using Equations (2.6) and (2.7), the angle of rotation for the glass plate will be calculated by θ_2-θ_1 [8].

2.2.5 Tilt Measurement using the Fabry-Perot Etalon

A Fabry-Perot etalon is typically made of a transparent plate with two reflecting surfaces. As is shown in Fig. 2.8, interference happens between the multiple reflections of light between the two reflecting surfaces. Constructive interference occurs if the transmitted beams are in phase and destructive interference happens if they are out-of-phase. Whether the multiply-reflected beams are in-phase or not depends on λ the wavelength of the light, θ the angle the light incident on the etalon, l, the thickness of the etalon and n, the refractive index of the material between the reflecting surfaces [7].

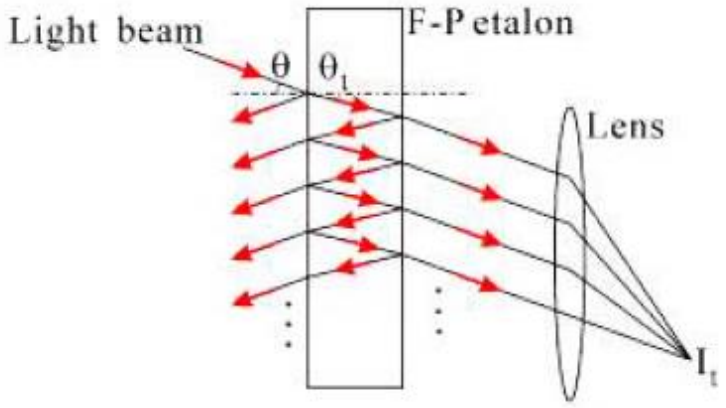

Figure 2.8 The Fabry-Perot etalon *[7]*.

This schematic of the angle measurement was proposed by Lin et al. and is shown in Fig. 2.9 [7]. Here the first PBS splits the linearly polarized laser beam equally into two beams, L_1 and L_2 which are both linearly polarized as well. These two beams pass through the Fabry-Perot etalon, which is on a rotational stage driven by a piezo actuator that is controlled by a computer, and then go through the second PBS, which directs L_1 and L_2 to the photo detectors PD_1 and PD_2 [7]. When the etalon is rotated the two beams suffer a phase shift which can be detected and related to the rotation. The accuracy in measuring rotation with this set up is 0.01 arc-sec.

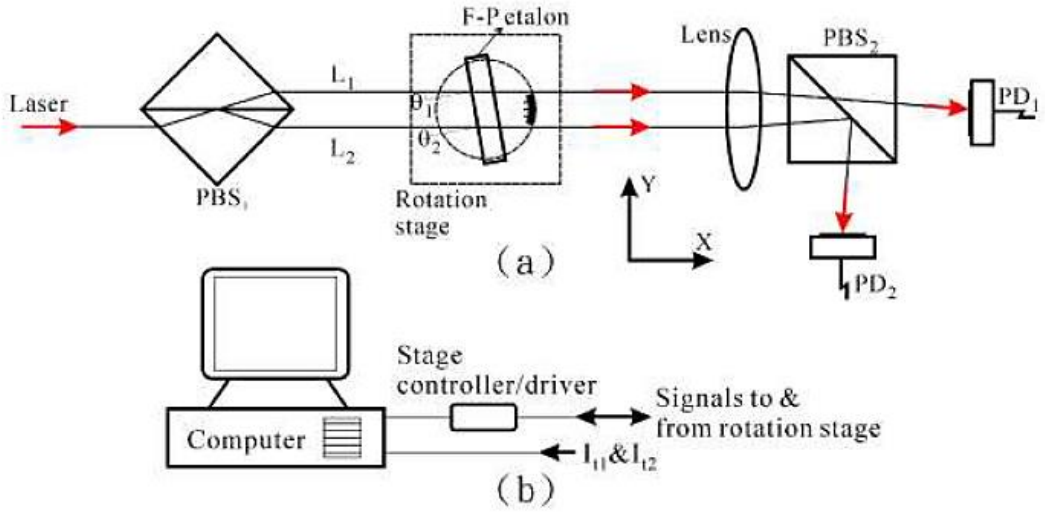

Figure 2.9 a) Schematic of the Angular probe and b) the control and signal processing system *[7]*.

2.3 Autocollimation technique for Measuring Small Tilt Angles

An Autocollimator, shown in Fig. 2.10, projects a collimated beam, which is completely or partially reflected by an external reflector back into the system, where it is then focused and detected by a photo detector. When the reflector is rotated, the focused spot shifts. From this shift, the rotation angle can be determined [21].

.

The autocollimator is simple and easy to work with but to achieve a high sensitivity there is a problem. The amplification factor is given by the ratio between the effective focal length of

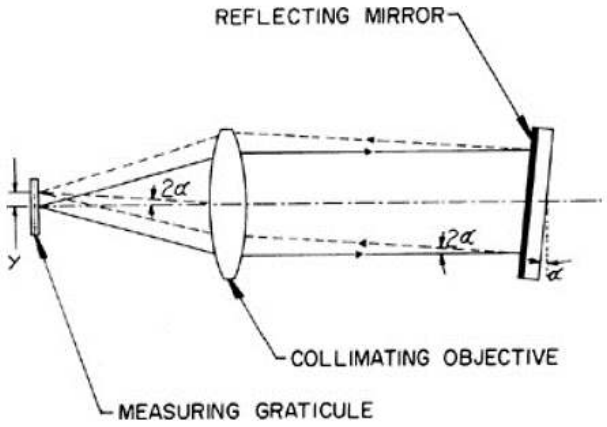

Figure 2.10 Schematic of an Autocollimator *[21]*.

the system and spatial resolution of the photo detector. A high sensitivity requires a long focal length. For example, an autocollimator having a focal length of 50 cm and a sensitivity of 5 nanoradians, needs a detector with a resolution and mechanical stability of 2.5 nm [21].

Pisani and Astrua proposed a method using multiple reflections that can help increase the sensitivity [22].

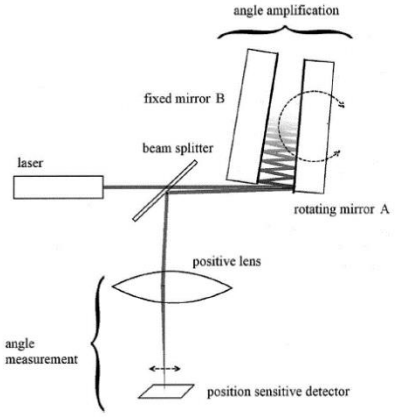

Figure 2.11 Schematic of the experimental setup for amplifying angle measurement using an Autocollimator *[22]*.

The schematic of their setup is presented in Fig. 2.11 which consists of a laser source, the angle amplification mirrors, and a device for measuring the angle. The laser source produces a collimated beam, the beam goes through a BS and is split into two beams, one goes towards the detector while the other hits mirror A, which is then reflected towards mirror B and bounces between the two mirrors approximately 60 times before exiting the mirrors and going back to the BS, which is reflected towards the angle measurement device. The angle measurement device includes a positive lens and a position-sensitive detector placed at the focal point of the positive lens [22].

3 Phase Shifting Method for Tilt Measurement in Cyclic Path Interferometer

In this chapter, the theory of tilt measurement in a cyclic path interferometer will be discussed. In addition, a different method of extracting phase information from the fringes using phase stepping methods will be discussed. Two methods of extracting phase namely the standard four-phase step and the phase differentiation method will be outlined.

3.1 Cyclic Path Interferometer

The setup for tilt measurement with a cyclic path interferometer is shown in Fig 3.1. Kumar et al. using their setup for measuring small tilt angles were able to measure angles as small as 23 arcsec (0.1mrad). The setup with three mirrors (rectangular cyclic path interferometer) is found to be twice as sensitive as a classical Michelson interferometer. As stated before since the two counter propagating beams travel identical paths, the interferometer is insensitive to external

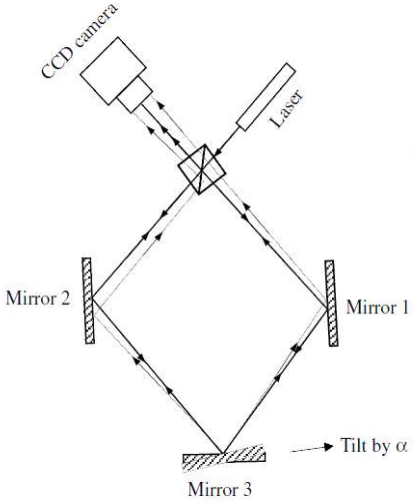

Figure 3.1 Schematic of the cyclic path interferometer with 4 mirrors, mirror 3 is the mirror that is tilted *[10]*.

vibrations and turbulences. The schematic diagram for this interferometer is shown in Fig. 3.1 [10]. A 50/50 beam splitter is used to generate two equal amplitude beams. Both beams travel the same path but in opposite direction. After traversing, the two beams recombine at the beams splitter where they interfere, Mirrors 1 and 2 are fixed while, mirror 3 introduces the tilt. By tilting Mirror 3, the two beams go through slightly different paths, thus causing a linearly increasing or decreasing phase change in the plane of the wavefront, which causes fringes of equal inclination to appear in the overlapping area. The path difference caused by the tilt in the case of a cyclic interferometer in both beams are equal but have different signs, positive for one and negative for the other. Thus the total path difference between the two beams is added and is twice that of a Michelson interferometer.

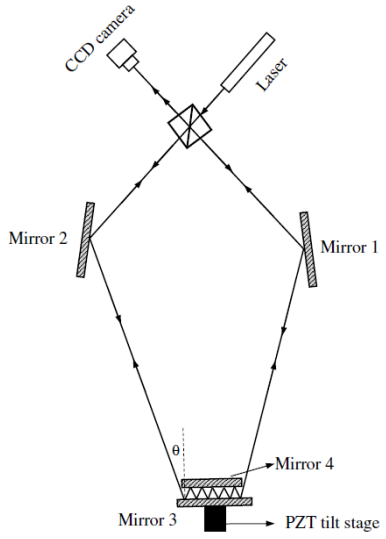

Figure 3.2 Schematic of the Cyclic path interferometer with multiple reflections *[10]*.

In order to increase the sensitivity of the system in measuring tilt angles a new system was described where the two beams are multiply reflected between two parallel mirrors. The modified schematic arrangement with the multiple reflection setup is shown in Fig. 3.2.

In the modified setup Mirror 3 has been replaced with a two-parallel mirror arrangement where Mirror 3 is mounted on a nano rotational stage. As the beams arrive at Mirror 3, they start to reflect between Mirror 3 and 4. After going through a series of multiple reflections, the beams leave the Mirror 3 and Mirror 4 assembly and recombine again at the BS. The number of multiple reflections increases the tilt sensitivity by a factor of 2N, where N is the number of reflections occurring on Mirror 3.

3.2 Theory of Multiple Reflections

As shown in Fig. 3.3, according to the basic law of reflection in geometrical optics, when a ray of light is incident on a flat mirror with an angle of α, the beam will be reflected from the surface of the mirror with an angle of α. If the mirror is rotated by an angle θ, the reflected beam will be rotated with an angle 2θ [22].

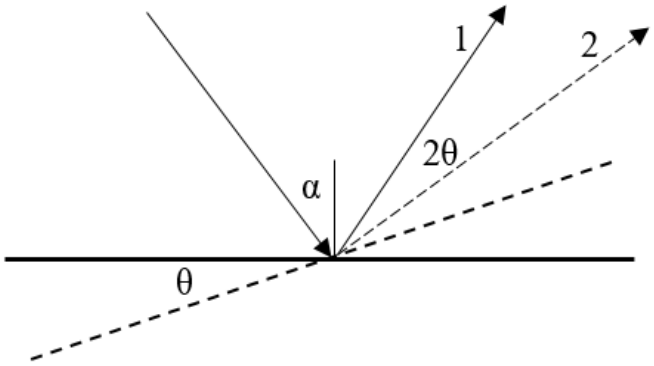

Figure 3.3 Effect of rotation of a mirror on reflecting beams.

In the case of two parallel flat mirrors, for example, Mirror3 and Mirror4 in Fig 3.4, when

a beam impinges on Mirror 3 with an angle of α it starts to bounce a few times between the two mirrors and at last it will exit with the same angle α. If Mirror 3 is rotated by an angle of θ,

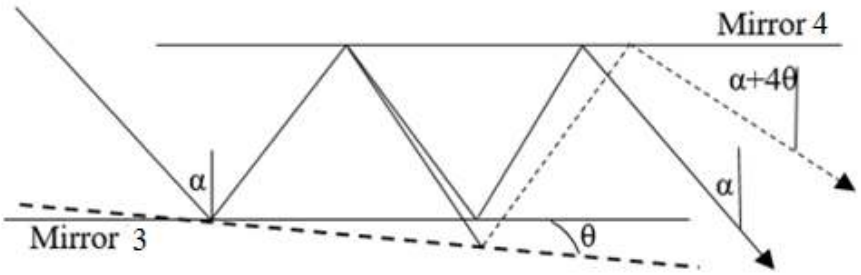

Figure 3.4 Effect of rotation of one of two mirrors in a setup with flat parallel mirrors.

where θ is much smaller than (θ << α), then after one reflection, the angle α will have doubled, similar to the case with one mirror. After each reflection of the beam, the angle doubles. Thus the beam which comes out of the system is eventually rotated with an angle 2Nθ, which N is the number of reflections on Mirror 1 (the tilted mirror) [22].

3.3 Multiple Reflection in Cyclic Path interferometer

As mentioned before, in the cyclic path interferometer, both beams travel the same distance before recombining at the beam splitter. As was shown in Fig. 3.2, to generate more reflections between Mirror3 and Mirror4, the angle θ, i.e., the angle between the beams as they enter and exit Mirror3, should be as small as possible. The relationship between the distance between the two mirrors (*d*), the length of Mirror 3 (*L*), the incident angle (θ) and the number of reflections (*N*) is as follows [10].

(3.1)

$$N = \frac{1}{2d} \cdot \frac{L}{\tan(\theta)}$$

That is, the number of reflections is inversely related to the incident angle and the distance between the mirrors, even though *N* increases with the length of Mirror 3. In order to make the beam enter the mirrors easily Mirror 3 is slightly longer than Mirror 4.

Assuming that the two beams reunite at the BS, where interference happens, *Z* is the distance between a virtual point behind Mirror3 and the BS. When no tilt is introduced to the system, the two beams will coincide at the BS but when Mirror 3 is tilted by an angle α, the centers of the two beams will be separated by a distance AB as shown in Fig. 3.5. In this case, if *X* is the distance between the center of the beam to any point on the beam, the optical path difference between the two beams at the small-angle condition can be calculated using Equation (3.2) [10].

$$OPD = 4XN\alpha \tag{3.2}$$

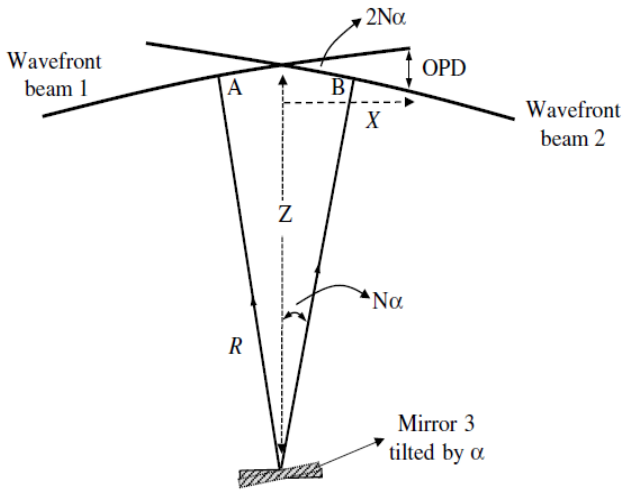

Figure 3.5 The effect of tilt on the beams in the cyclic path interferometer proposed by Kumar et al.

If the beam is close to being collimated, then the radius of curvature of the beam does not affect the fringe spacing. The tilt angle then can be calculated using Equation (3.3). In this equation, it has been assumed that the wavefront is aberration free. Further studies of the influence of aberrations on the tilt measurement were carried out and shown that spherical aberration will introduce large errors in the measurement of tilt [23].

$$\alpha = \frac{\varphi}{2\pi} \cdot \frac{\lambda}{4XN} \tag{3.3}$$

3.4 Different Methods for Evaluating Phase in the Cyclic Path Interferometer

There are three possible ways to measure the fringe spacing observed in the overlapped region of the cyclic interferometer. The first method is a basic method using fringe tracing, where the fringes are thinned and the spacing between them is evaluated. In the second method, when relatively large number of fringes are obtained, a Fourier transform method can be used to extract the total phase and thereby the tilt. A third and robust method is to employ a phase stepping routine to extract the phase. The previous work [10], used another method by assuming that the fringes formed are of unit visibility cosine squared ($\cos^2$) plot was fit to the fringes and the phase was extracted. In the case of fringes with lower visibility a constant intensity value was subtracted and then the fringes were fit with the cosine squared profile. However, the drawback of this evaluation is that there must at least one fringe in the field, which places a natural lower bound on the smallest tilt angle that can be measured by this method. In this thesis, polarization phase stepping was used to extract the phase the limit was lowered from micro radians to nanoradians [10].

3.4.1 The Fringe Tracing Method

In this method, positions of the individual fringes are detected and used as interpolation points. This is because the phase value for each fringe is known at least relatively to other fringes. Points along a fringe all have the same phase value while the phase difference between adjacent fringes is known to be 2π. In the next step, the intermediate phase values between the fringes are interpolated using the fringe values at the center as interpolation points. In the fringe tracing method, there is still error in detecting the center of the fringes despite the method's use of computers, which causes a decrease in the accuracy of the phase. A diagrammatic explanation of the process is shown in Fig. 3.6.

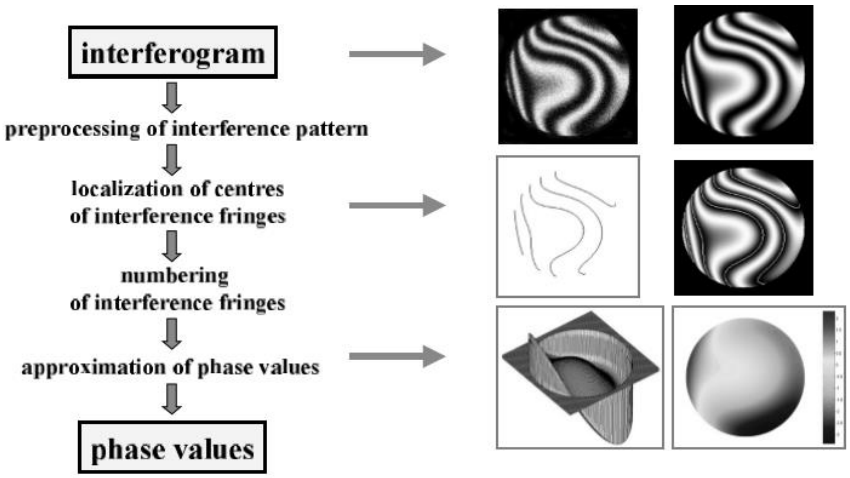

Figure 3.6 Process of phase evaluation using the fringe tracking method *[24]*.

3.4.2 The Fourier Transform Method

This method is based on the Fourier transform of the intensity distribution of the interferogram pattern. In this method, when the fringes are oriented along one direction such that the carrier signal of higher frequency is modulated by a low frequency original signal, then a one-dimensional Fourier transform along a line perpendicular to the fringes can be performed. Figure

3.7 shows a diagrammatic explanation of this process where one can see that the original fringes have a high carrier fringe overlaid by a low frequency signal [24].

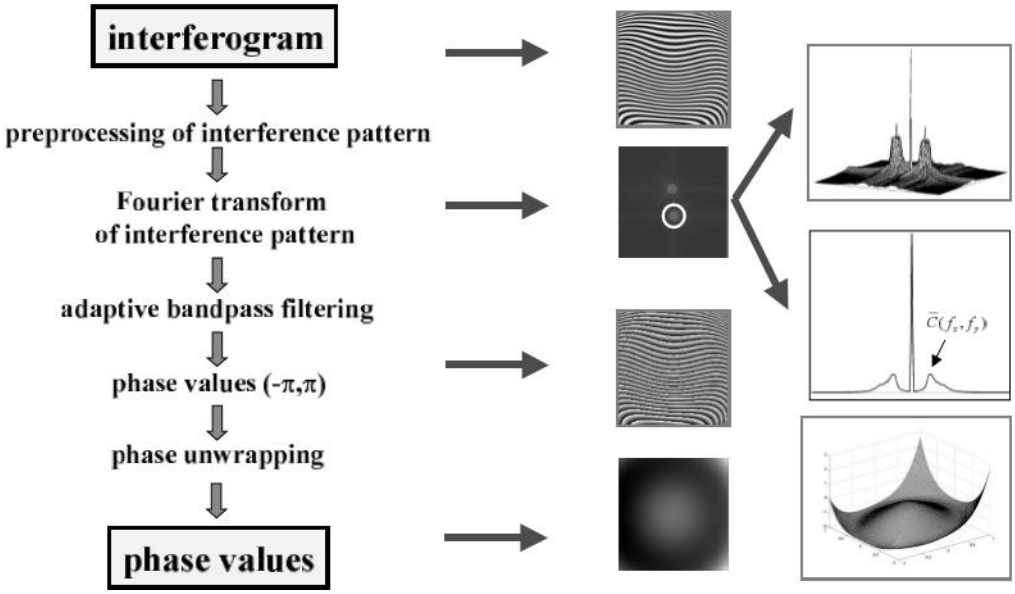

Figure 3.7 Process of phase evaluation using the Fourier transform method *[24]*.

The Fourier transform produces a central maximum and two side order peaks that carry the low frequency signal. A bandpass filter is then used to isolate one-of-the side band in the Fourier spectrum. This side band is then centered and the phase information is extracted by performing an inverse Fourier transform.

3.4.3 Phase Shifting Method

In order to extract quantitative data from an interference pattern, the phase difference between the two interfering beams must be extracted. In this method, a known phase difference is introduced between the two beams in a few steps. After each step, the image of the interference pattern is recorded. With a known phase shift, it is then possible to calculate the original phase difference between the interfering beams. There are many algorithms that have been developed in

the literature to accomplish this task and the most commonly used method is the four-phase step method. The data from this algorithm will be used to calculate the primary phase difference between the interfering beams [6]. The phase stepping method has a lot of advantages compared to other techniques:

- High measurement accuracy
- Rapid measurement
- Good results with low contrast fringes
- Results independent of intensity variations across pupil

There are two types of phase stepping techniques used in interferometry namely temporal phase step and spatial phase step. In this thesis, the focus has been primarily on the temporal phase step using a polarization phase stepping technique. There are different methods that have been developed to introduce the constant phase step and this is discussed in the following sections.

3.3.3.1 Phase Shifting - Moving Mirror

By far the most common method used to introduce a time-varying phase shift in a phase

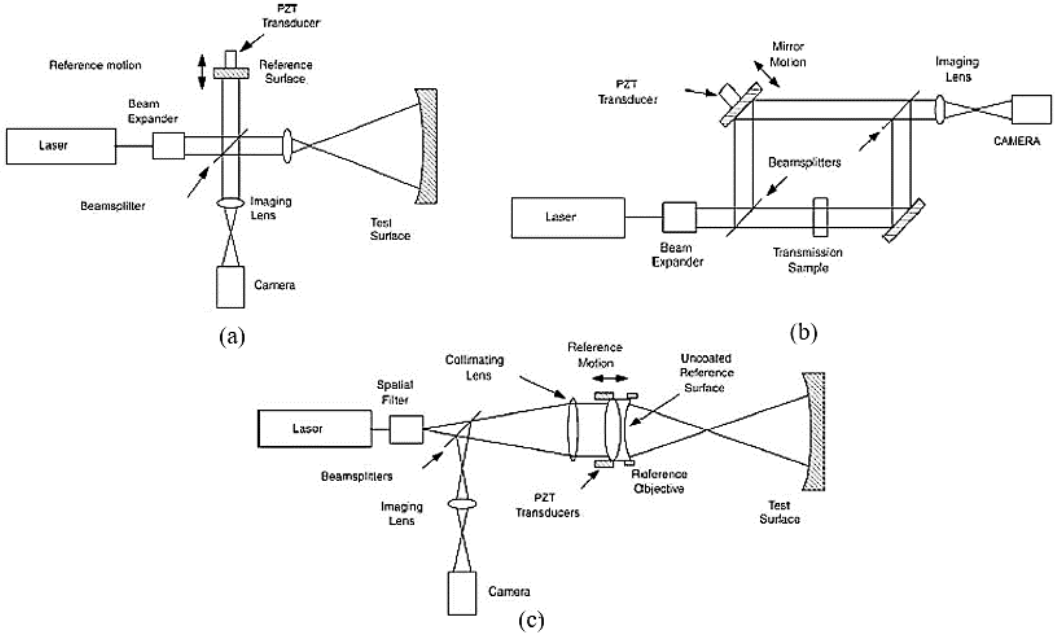

Figure 3.8 Three common interferometer configurations: (a) Twyman-Green, (b) Mach-Zehnder, (c) Fizeau [6].

shifting interferometric system is to translate one of the mirrors or optical surfaces in the interferometer with a piezo electric transducer (PZT). Depending on the configuration of the PZT, up to a few hundred volts may be needed to obtain the required motion of a wavelength or less. By discretely changing the applied voltage, the required phase shift can be introduced.

If the voltage is programmed to vary smoothly, a phase shift of a desired functional form can be produced. This method has been used in different interferometers such as the Twyman-Green, The Mach-Zehnder and the Fizeau interferometers as shown in Fig. 3.8 [6].

3.3.3.2 Phase Shifting - Diffraction Grating

When a diffraction grating is translated through a beam of light, a Doppler shift is introduced in the diffracted beams. The translation direction is perpendicular to the propagation

direction. The frequency shift is proportional to the diffraction order m and the velocity v, and inversely proportional to the grating period d, or

$$\Delta v = \frac{mv}{d} \tag{3.4}$$

The un-diffracted beam has no frequency shift, beams diffracted in the same direction as the translations see a positive frequency shift while beams diffracted in the opposite direction have their frequency decreased. One of the diffracted orders is selected and interfered with the original frequency to produce a phase shifting interferometer [25].

3.3.3.3 Polarization Phase Shifting

In polarization phase shifting, generally, the reference and test waves with linear orthogonal polarizations are transformed to opposite circular polarizations and are allowed to pass through a linear polarizer. The (geometrical) phase shift is introduced by varying the angular orientation of the pass direction of the polarizer. Polarization phase shifting has been applied to different interferometric configurations [25].

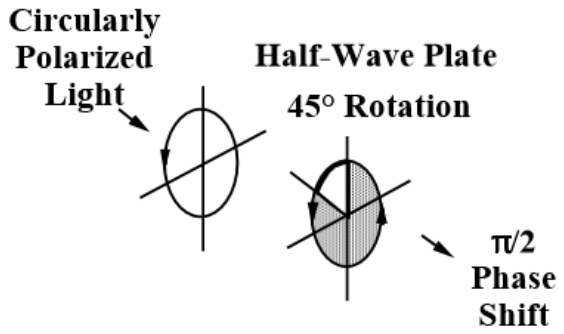

Figure 3.9 Polarization Phase shifter arrangements [25].

The most important advantage of this method is that it allows one to capture all the necessary phase-shifted interferograms simultaneously, thereby reducing the vibration susceptibility to a minimum and extending the scope of the measurement to dynamic interferometry.

3.4.4 Detecting the Wavefront Phase

After introducing the phase shift into the system there are several algorithms used to calculate the phase shift introduced in the system. In the following sections, two methods that have been used for measuring tilt will be discussed.

3.3.4.1 The Four-Step Algorithm with Constant Visibility

The easiest algorithm, introduces the phase shift in 3 steps resulting in 4 measurements [6]. The phase difference introduced in each step is π/2. If the phase shift introduced into the system is δ and has four values as follows:

$$\delta_i = 0, \frac{\pi}{2}, \pi, \frac{3\pi}{2}; i = 1,2,3,4$$

Substituting these values for δ in equation (3.5)

$$I(x,y,t) = I'(x,y) + I''(x,y)\cos(\varphi(x,y) + \delta(t)) \quad (3.5)$$

Where I' is the average intensity and I'' is the fringe or intensity modulation. Assuming that with the introduction of phase step, there is no change in the visibilities of the fringes. The result will be as shown in equations (3.6) to (3.9) as follows:

$$I_1(x,y,t) = I'(x,y) + I''(x,y)\cos(\varphi(x,y)) \tag{3.6}$$

$$I_2(x,y,t) = I'(x,y) + I''(x,y)\cos(\varphi(x,y) + \frac{\pi}{2}) \tag{3.7}$$

$$I_3(x,y,t) = I'(x,y) + I''(x,y)\cos(\varphi(x,y) + \pi) \tag{3.8}$$

$$I_4(x,y,t) = I'(x,y) + I''(x,y)\cos(\varphi(x,y) + \frac{3\pi}{2}) \tag{3.9}$$

Using trigonometric identities will result in:

$$I_1(x,y,t) = I'(x,y) + I''(x,y)\cos(\varphi(x,y) \tag{3.10}$$

$$I_2(x,y,t) = I'(x,y) - I''(x,y)\sin(\varphi(x,y)) \tag{3.11}$$

$$I_3(x,y,t) = I'(x,y) - I''(x,y)\cos(\varphi(x,y)) \tag{3.12}$$

$$I_4(x,y,t) = I'(x,y) + I''(x,y)\sin(\varphi(x,y)) \tag{3.13}$$

By solving these four equations with three unknowns, the value of φ will be calculated for each point on the interferogram. The calculation can be done only by using three images, but the fourth one is included in order to make the calculation easier. How these equations are solved for φ is shown in equations (3.14) to (3.17).

$$I_4 - I_2 = 2I''(x,y)\sin(\varphi(x,y)) \tag{3.14}$$

$$I_1 - I_3 = 2I''(x,y)\cos(\varphi(x,y)) \tag{3.15}$$

By taking the ratio of (3.19) and (3.20), term *2I″* is eliminated, leaving us with the following:

(3.16)

$$\frac{I_4 - I_2}{I_1 - I_3} = \frac{\sin(\varphi(x,y))}{\cos(\varphi(x,y))} = \tan(\varphi(x,y))$$

This will lead us to the amount of phase difference between the two interfering beams

$$\varphi(x,y) = tan^{-1}\left(\frac{I_4 - I_2}{I_1 - I_3}\right) \tag{3.17}$$

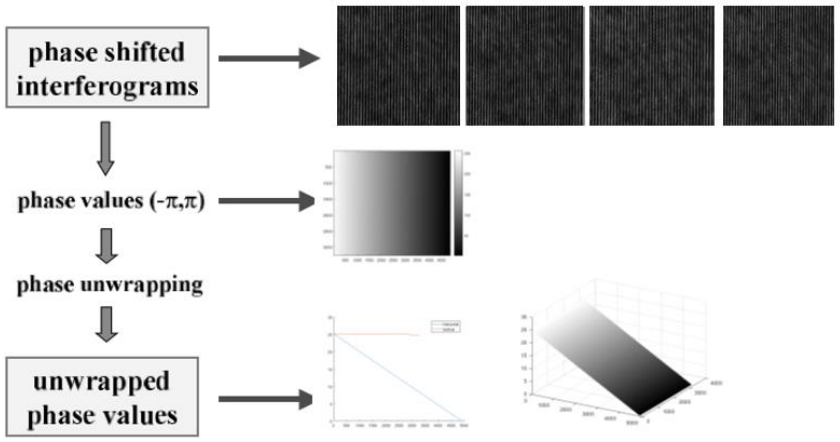

Figure 3.10 Process of phase evaluation using phase shifting.

A diagrammatic explanation of how the four-phase step method works is shown in Fig. 3.10. It is worth mentioning that there are several algorithms used to measure the phase difference using the phase shifting method. These algorithms vary in the number of phase steps they employ, from one all the way to five [26].

3.3.4.2 Phase differentiation Method with Constant Visibility

This method works like the Phase Shifting method but the difference is that only two steps of a known value are required [27]. The equation for the interference between the reference and the test wavefront is as follows:

$$I_1(x, y, t) = I_0\{1 + \gamma cos(\delta(x, y))\} \tag{3.18}$$

In Equation 3.21, $I_0$is the average intensity, γ is the visibility of the interference pattern, and $\delta(x, y)$ is the wavefront phase. In the next step, a phase shift of π/2 is introduced into one of the beams, the result of which will be the second interference pattern with an intensity of:

$$I_2(x, y, t) = I_0\{1 - \gamma sin(\delta(x, y))\} \tag{3.19}$$

It has been mentioned that any value of phase step can be introduced into the system in order to generate the second interference pattern. Joenathan and Khorana [27] used a phase step of π/2 for simplicity of calculations. Each of the phase stepped interference fringes are sheared by a few pixels along the y or x direction, which depends on the slope of the wavefront. If the shear has to be along one direction, this can be done by introducing a known amount of tilt between the interfering beams [27].

The equations for the differential intensity data for the case that the tilt is along the x axis, can be expressed as:

$$I_1^d = I_1(x + \Delta x, y) - I_1(x, y) = I_0\gamma\{\cos(\delta(x + \Delta x, y)) - cos(\delta(x, y))\} \tag{3.20}$$

And

$$I_2^d = I_2(x + \Delta x, y) - I_2(x, y) = -I_0\gamma\{\sin(\delta(x + \Delta x, y)) - sin(\delta(x, y))\} \quad (3.21)$$

Which Δx is the lateral displacement of the fringe pattern. By using the Taylor series, equations 3.22 and 3.23 can be simplified into the following equations:

$$I_1^d = -I_0\gamma\{\sin(\delta')[\sin(\delta(x, y))]\} \quad (3.22)$$

And

$$I_2^d = -I_0\gamma\{\sin(\delta')[\cos(\delta(x, y))]\} \quad (3.23)$$

Which $\delta' = (\partial\delta(x, y)/\partial x)\Delta x$ where $\partial\delta(x, y)/\partial x$ is the slope of the phase function. Therefore, the phase at the point (x, y), can be calculated by dividing equation 3.22 by 3.23:

$$\delta(x, y) = tan^{-1}\left(\left[\frac{I_1^d}{I_2^d}\right]\right) \quad (3.24)$$

3.3.4.1 Phase differentiation Method with Varying Visibility:

In the cyclic interferometer because the beams travel the same path, the conventional method of moving the mirror or grating or stretching the fiber cannot be used and the phase shift will occur in both the beams. Thus, the resultant phase difference will always be zero. Therefore, a new and simple phase step method using polarization was developed. Since a linear polarization beam is converted into a circularly polarized beam using a quarter-wave plate, the chances of getting perfect circular polarization is hard. Also, the rotation of a half-wave plate converts the circularly polarized light into a linear polarized beam that will interfere when they combine at the Beam Splitter. The phase shift is introduced by rotating the half-wave plate in steps of 45 degrees.

This can cause changes in the amplitudes of the two counter propagating beams, and thus there is a possibility of a change in the visibility of the fringes.

To overcome this problem, a new method of phase evaluation using the phase differentiation method was introduced. If $I_0$is the average intensity and γ is the visibility of the interference pattern and $\delta(x,y)$ is the wavefront, the equation for the interference between the reference and the test wavefront is as follows:

$$I_1(x,y) = I_0\{1 + \gamma_1 cos(\delta(x,y))\} \tag{3.25}$$

A phase shift of π radians is introduced, and a second image of the interference pattern is captured. Do note that a phase shift of π is introduced by rotating the half-wave plate by π/2. The amplitudes of the resulting linearly polarized light can vary, thus causing a change in the fringe visibility. It must be noted that the average intensity or the bias might not change very much in the process. The equation for the interference with the phase shift become

$$I_2(x,y) = I_0^2\gamma_2\{1 - \gamma_2 cos(\delta(x,y))\} \tag{3.26}$$

$$I_2(x,y) - I_1(x,y) = I_0' - I_0 - \cos(\delta(x,y))\{I_0^1\gamma_1 + I_0^2\gamma_2\} \tag{3.27}$$

By approximating that I_0' and I_0 are equal equation 3.27 will become

$$I_1(x,y) - I_2(x,y) = \cos(\delta(x,y))\{I_0^1\gamma_1 + I_0^2\gamma_2\} \tag{3.28}$$

$$\frac{I_1(x+\Delta x) - I_1(x)}{\Delta x} = I_0^1\gamma_1 \sin(\delta(x,y)) \tag{3.29}$$

$$\Delta I_1 = I_1(x+\Delta x) - I_1(x) = I_0^1\gamma_1 \sin(\delta(x,y))\Delta x \tag{3.30}$$

Which Δx is the lateral displacement of the fringe pattern.

$$I_0^1\gamma_1 = \frac{\Delta I_1}{\sin(\delta(x,y))\Delta x} \tag{3.31}$$

$$\Delta I_2 = I_2(x+\Delta x) - I_2(x) = -I_0^2\gamma_2\sin(\delta(x,y))\Delta x \tag{3.32}$$

$$I_0^2\gamma_2 = -\frac{\Delta I_2}{\sin(\delta(x,y))\Delta x} \tag{3.33}$$

By substituting equations 3.31 and 3.33 into equation 3.28 the result will be:

$$I_1(x,y) - I_2(x,y) = \cos(\delta(x,y))\left\{\frac{\Delta I_1}{\sin(\delta(x,y))\Delta x} - \frac{\Delta I_2}{\sin(\delta(x,y))\Delta x}\right\} \tag{3.34}$$

$$I_1(x,y) - I_2(x,y) = \cot(\delta(x,y))\left\{\frac{\Delta I_1}{\Delta x} - \frac{\Delta I_2}{\Delta x}\right\} \tag{3.35}$$

At last:

$$\left\{\frac{\Delta I_1}{\Delta x} - \frac{\Delta I_2}{\Delta x}\right\} = \tan\big(\delta(x,y)\big)\{I_1(x,y) - I_2(x,y)\} \tag{3.36}$$

$$\delta(x,y) = tan^{-1}\left[\frac{\Delta I_1 - \Delta I_2}{(I_1 - I_2)\Delta x}\right] \tag{3.37}$$

Do note that the maximum value of phase obtained using equations 3.17 and 3.24 is 2π. Therefore, the phase map will cycle between 0 to 2π, which is called the raw phase map. To obtain the phase, the raw phase map needs to be unwrapped; i.e., the 2π phase ambiguities need to be removed.

Here, the phase unwrapping code obtains the maximum value of the phase along the x-and y-directions in order to determine the tilt of the mirror using the cyclic interferometer. In this thesis, the Polarization Phase shifting was used, and the phase was calculated using both algorithms introduced in this chapter.

4 Experimental Work

The goal of this thesis is to measure small tilt angles in the order of nanoradians with high accuracy using a cyclic path interferometer.

4.1 Experimental Setup

The schematic of the initial setup of the cyclic path interferometer is shown in Fig. 4.1. A He-Ne laser beam passes through a microscope objective, a pinhole and a collimating lens system. The spatial filtering is accomplished by using a microscope objective MOL and a pinhole PH combination that clean up the diverging laser beam. The laser beam is collimated after passing through the collimating lens placed in the path of diverging beam such that focal point of the

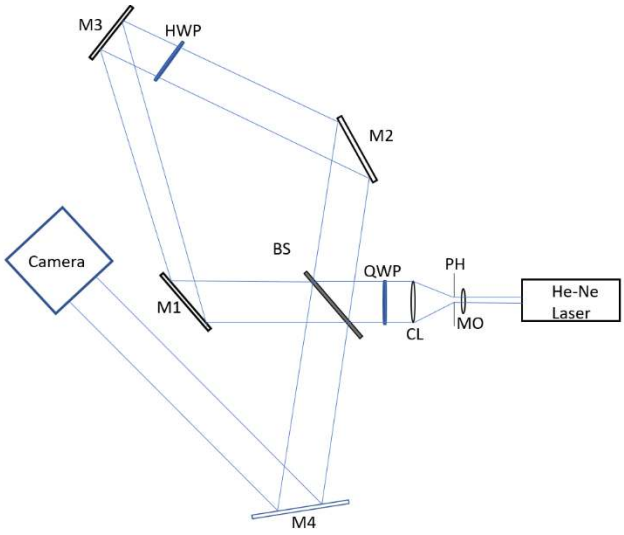

Figure 4.1 Schematic of the Setup for the cyclic path interferometer used in this thesis.

collimating lens coincides with the focus spot created by the microscope objective. The collimated beam is aligned to be parallel to the table.

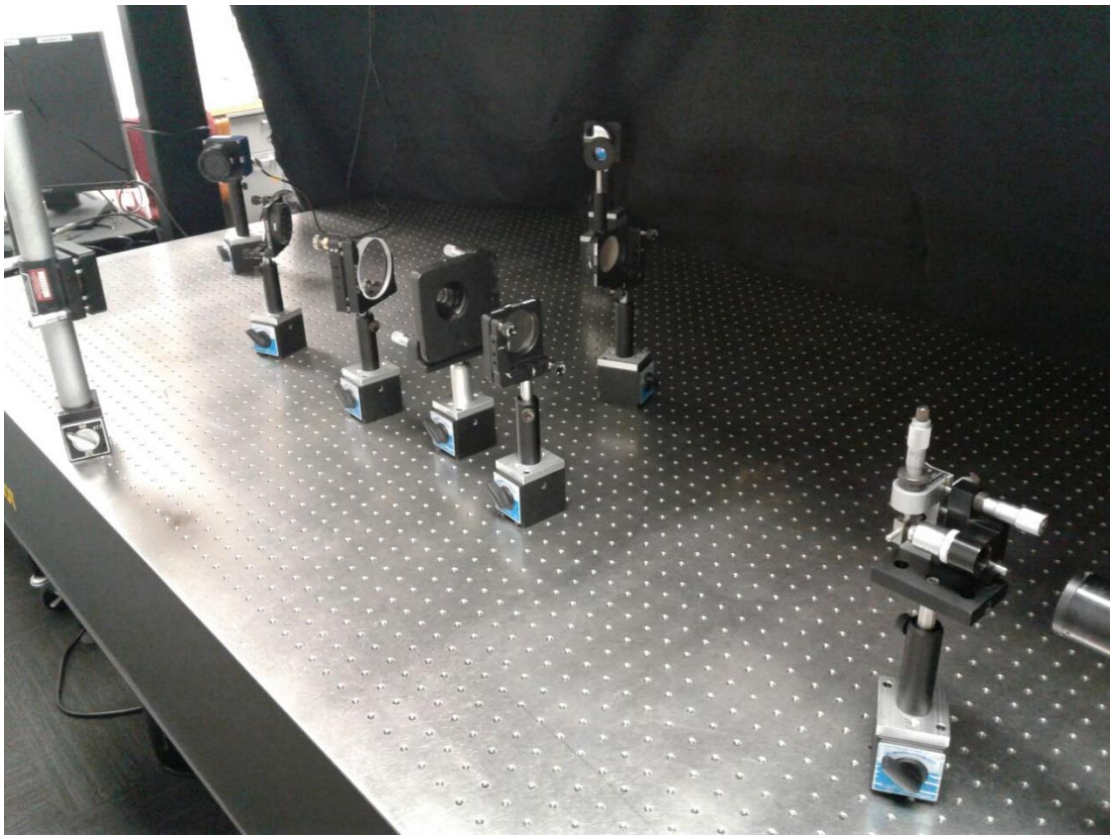

Figure 4.2 Photo of the experimental setup, before inserting the fourth mirror for multiple reflections.

In order to make sure that the beam doesn't converge or diverge as it propagates, a single fringe is created in a shear plate placed in the path of the beam. After making sure that the beam is very well collimated, the beam passes through a 50/50 BS. Beam1 goes through M_1, M_3, and M_2, while Beam2 goes through M_2, M_3, and M_1. They both meet again at the BS. The interference of the two beams is then recorded by a large pixel array camera. A photograph of the setup is shown in Fig. 4.2.

4.1.1 Alignment Procedure

1. Beam Collimation using shear plate.
2. Make sure arm lengths are the same.
3. Make sure beams go through the center of optical elements.
4. Make sure both beams meet at the same point on M2 (no fringes are observed in the region the beams overlap after the BS).
5. After making sure about the 4 steps above, the mirrors M1 and M3 are moved in a way that the fringes are observable.

4.2 Phase Evaluation

The goal of this work was to increase the measurement accuracy to tilt. It is well known that phase maps of the wavefront can be extracted using phase stepping routines and thus the focus was to develop a method to introduce a known phase step between the counter propagating beams. The traditional method of moving a mirror mounted on a PZT stage to introduce phase cannot be used here because any phase shift introduced in one beam will be identical to the phase step introduced in the counter propagating beam. It was found that the polarization phase step method will lend itself very easily to the cyclic interferometer. A simple, easy to implement, and novel method of phase step with fewer components has been introduced. The output of the laser beam is linearly polarized and then sent through a quarter-wave plate that converts the linear polarized light to circularly polarized light. In one of the arms of the cyclic interferometer, a half-wave plate is introduced that converts the circularly polarized light back to linear polarized light as it propagates in both directions. It is well known that the linear polarized light generated by the half-

wave plate is phase shifted based on the angle of rotation. Thus, a known amount of phase step can be introduced between the two beams by rotating the half-wave plate.

A half an inch diameter quartz quarter-wave plate was placed with its optic axis at an angle of 45o with respect to the incident laser beam's polarization orientation. At this angle, the linearly polarized light was converted to a right circularly polarized beam. A half inch diameter half-wave plate was then placed in one of the interferometer's arms. It did not matter which arm because both beams travel identical paths. As the half-wave plate was rotated, a phase shift was introduced between the two beams and a dynamic change in the fringes was observed. In the initial stages, it was observed that not only a phase shift was introduced, but there was also a slight change in the visibility of the fringe. The change in the visibility was reduced to zero by carefully aligning the quarter wave plate to get a perfectly circular polarized light. It was observed that, by rotating the half-wave plate, a small amount of tilt was introduced into the system also, thus making the fringe unstable as the half-wave plate was rotated. In order to reduce the tilt caused by the half-wave plate, it was mounted on an XYZ tilt stage to make the half-wave plate rotate perpendicular to the incident plane wavefront. At each step, the half waveplate was rotated by 22.5^{o}. Thus, at the end of four-step phase shift the achieved phase shift was 90^{o}.

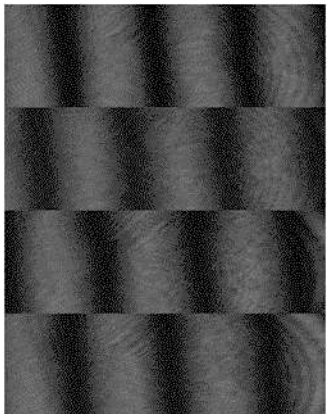

Figure 4.3 Pictures taken from the output fringes of the cyclic path interferometer using the four-step phase shifting method

In order to extract the phase of the wavefront, a series of images of the fringes were captured with a phase step of π/2 introduced after each exposure. Four such images were captured as the phase step cycled from 0 to 3π/2 in steps of π/2. The first method a four-step algorithm was used as discussed in section 3.3.4.1. The four images of the interference pattern phase shifted by π/2 are shown in Fig. 4.3. These images were then imported into a Matlab program that used the four-phase step algorithm to evaluate the phase. To reduce noise from spurious reflections and scattering, each image was processed with a 5x5 medium filter. The raw phase map, the

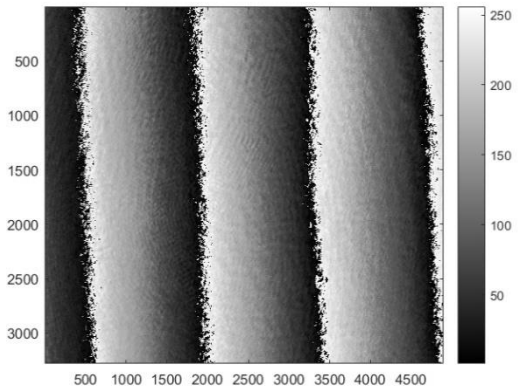

Figure 4.4 Raw image of the interferogram.

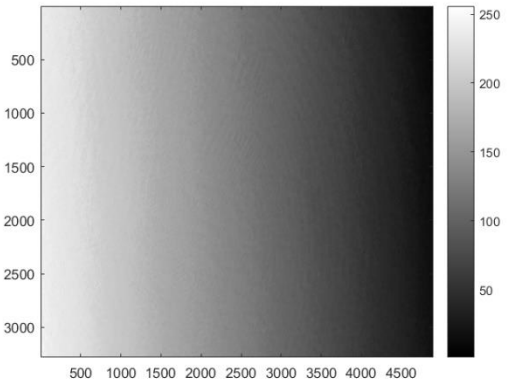

Figure 4.5 Phase map achieved using the four-step phase shifting algorithm.

unwrapping phase map and the phase plots achieved using the Matlab code is shown in Fig. 4.4, 4.5, 4.6 and 4.7 respectively.

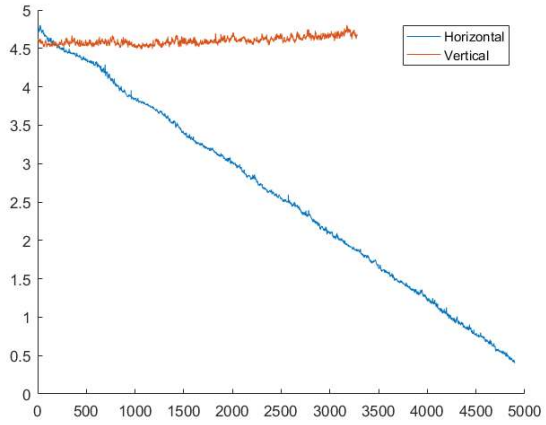

Figure 4.6 2D unwrapped phase plot for the four-step phase shifting method.

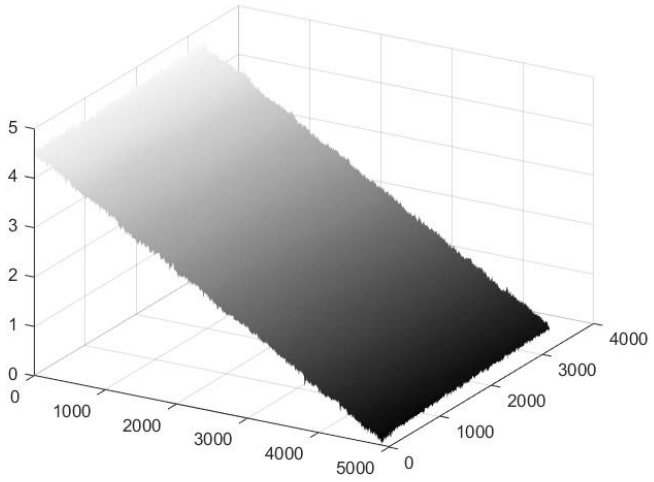

Figure 4.7 3D unwrapped phase plot for the four-step phase shifting method.

In order to reduce the number of phase steps, the phase was evaluated using the phase differentiation method. Since the phase is linearly increasing with position, the phase

differentiation method is a suitable and easy alternative to the four-phase step method. In addition, only two images of the fringes need to be captured with a phase step of $\pi/2$ between them.

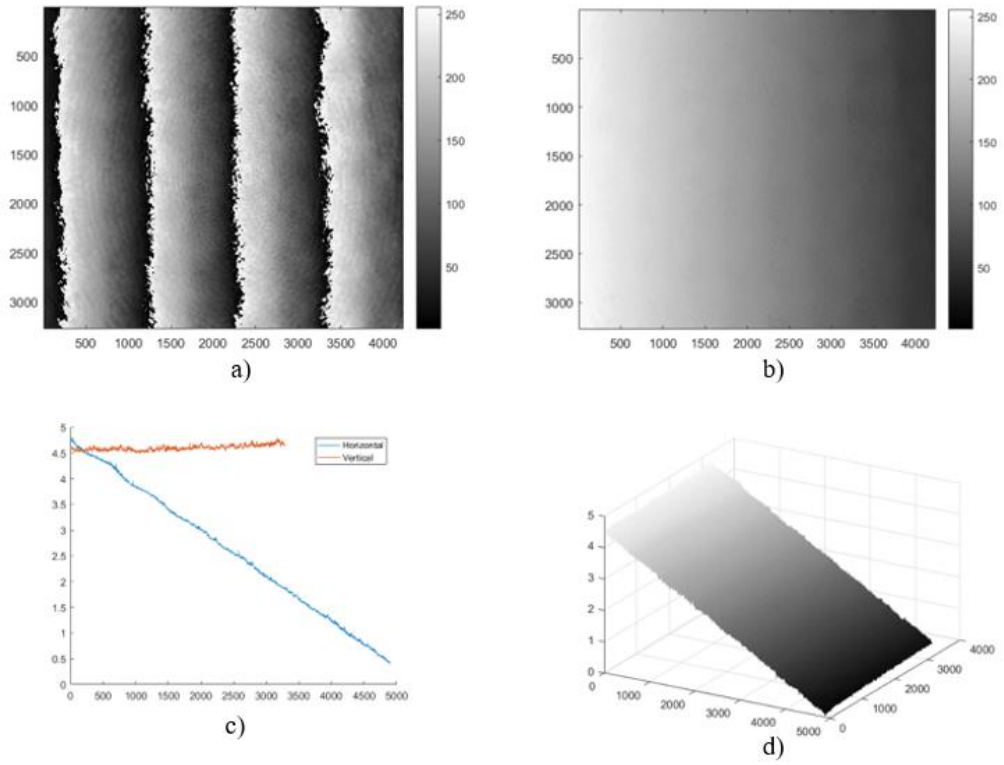

Figure 4.8 Results obtained with the phase differentiation method with a) the raw phase map, b) the unwrapped phase map, c) a line along the x and y axis passing through the center of the phase map, and d) the 3D plot of the tilted wavefront.

4.3 Quantitative measurement of tilt at the nanoscale using four-phase step method

In order to measure tilt at the nanoscale, a 50 mm flat mirror (M3 in Fig. 4.1) to be tilted was mounted on a Mad City Labs nano-tilt stage (Nano-MTA single axis). The tilt stage was then connected to a power supply from Mad City Labs to be able to give tilts with a resolution of 2

nanoradians. The maximum tilt that can be introduced in mirror M3 is 1 μrad. A known tilt of 1000 nanoradians was introduced in the cyclic interferometric arrangement of Fig 4.1. Using the four-phase step routine, four fringe patterns were captured, and the value of tilt was then automatically calculated using the total phase and the total width of the CCD camera along with the conversion equation:

$$\text{Measured tilt in radians} = \frac{(Phase_{max} - Phase_{min}) * \lambda}{\pi * pixelsize * number\ of\ horizontal\ pixels} * \frac{\pi}{180} \quad (4.1)$$

The tilt in Mirror M3 was gradually reduced in steps as follows: 1000, 500, 200, 50, 20, 5, and 2 nanoradians. The given tilt was then compared to the measured tilt using the cyclic interferometric fringes and four-phase stepping routine. Figures 4.9 to 4.16 shows the results for each other tilt angles.

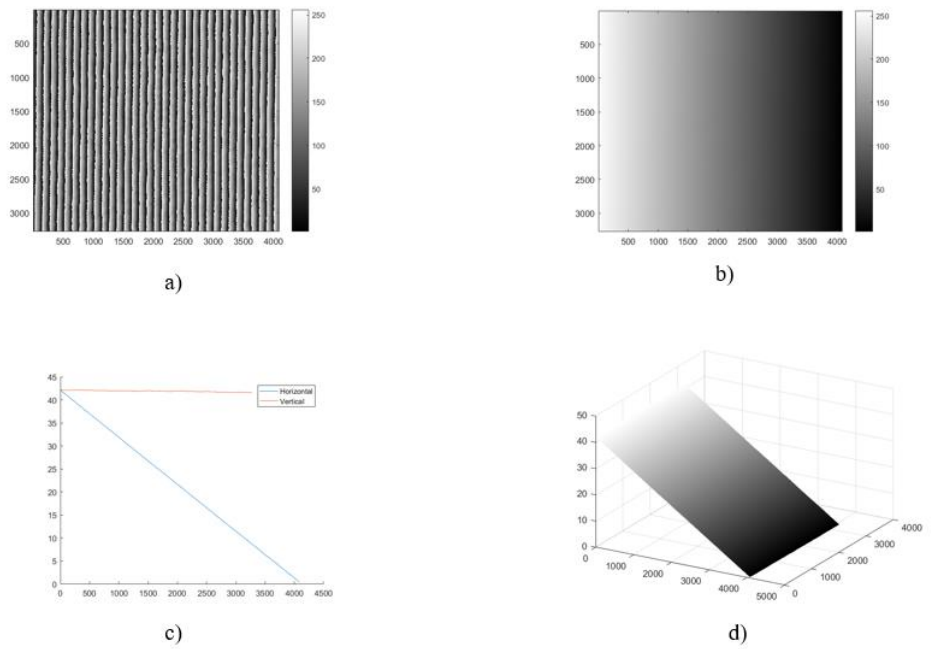

Figure 4.9 Result for 1000 nanorad tilt introduced into the system using four-step phase shifting method, a) raw image of the interference pattern, b) Phase map, c)2D unwrapped phase plot and d)3D unwrapped phase plot.

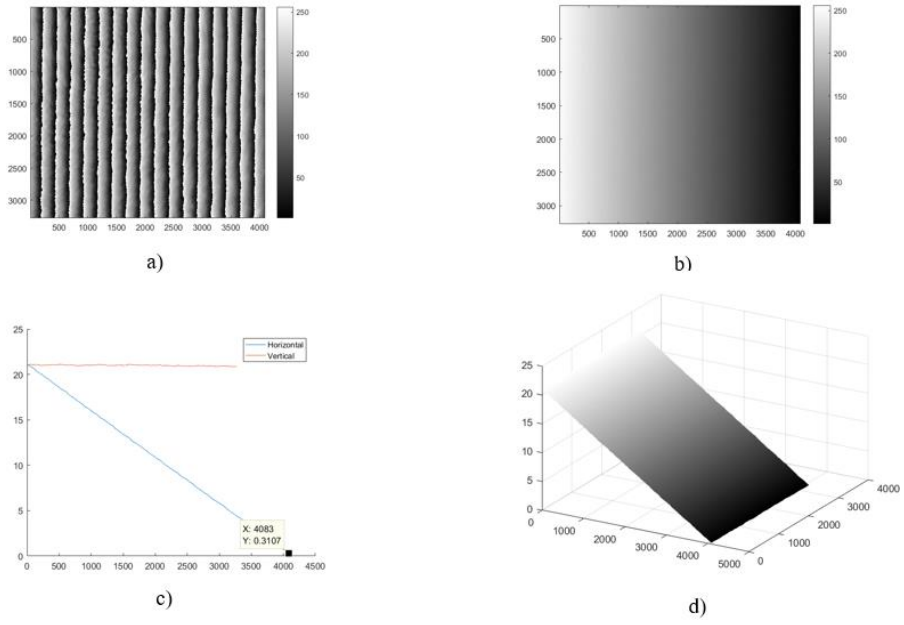

Figure 4.10 Results for 500 nanorad tilt introduced into the system using four-step phase shifting method, a) raw image of the interference pattern, b) Phase map, c)2D unwrapped phase plot and d)3D unwrapped phase plot.

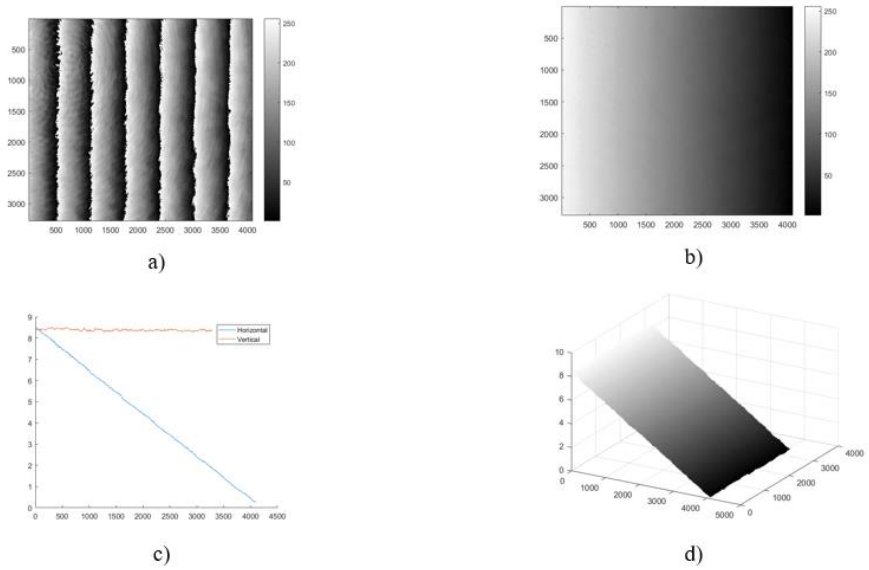

Figure 4.11 Results for 200 nanorad tilt introduced into the system using four-step phase shifting method, a) raw image of the interference pattern, b) Phase map, c)2D unwrapped phase plot and d)3D unwrapped phase plot.

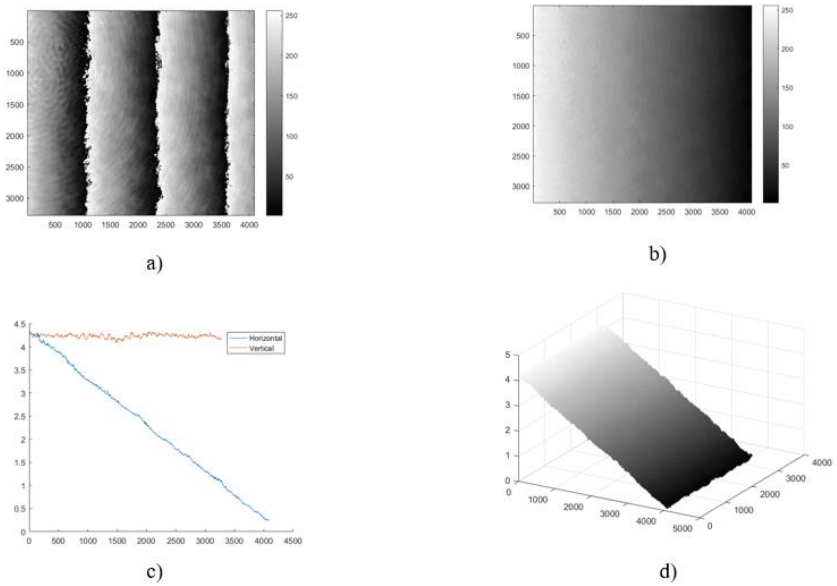

Figure 4.12 Results for 100 nanorad tilt introduced into the system using four-step phase shifting method, a) raw image of the interference pattern, b) Phase map, c)2D unwrapped phase plot and d)3D unwrapped phase plot.

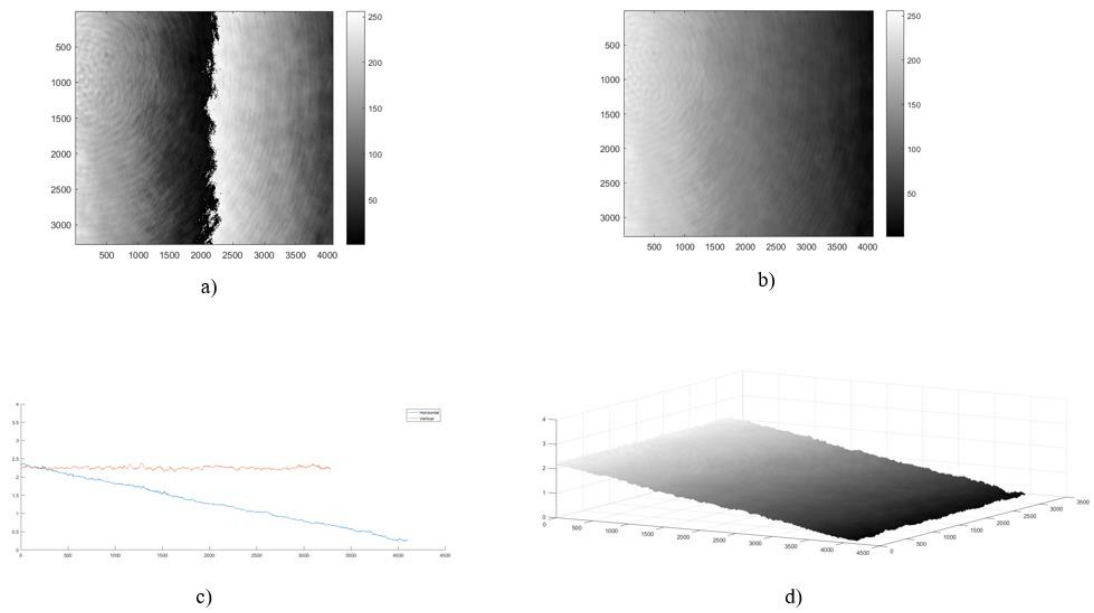

Figure 4.13 Results for 50 nanorad tilt introduced into the system using four-step phase shifting method, a) raw image of the interference pattern, b) Phase map, c)2D unwrapped phase plot and d)3D unwrapped phase plot

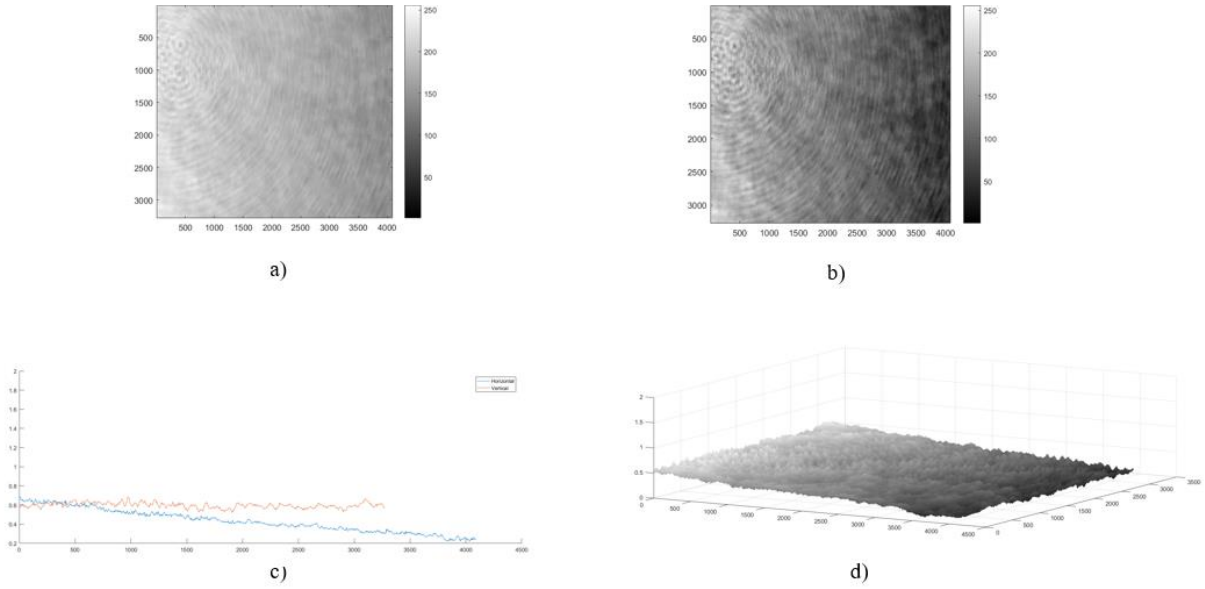

Figure 4.14 Results for 10 nanorad tilt introduced into the system using four-step phase shifting method, a) raw image of the interference pattern, b) Phase map, c)2D unwrapped phase plot and d)3D unwrapped phase plot

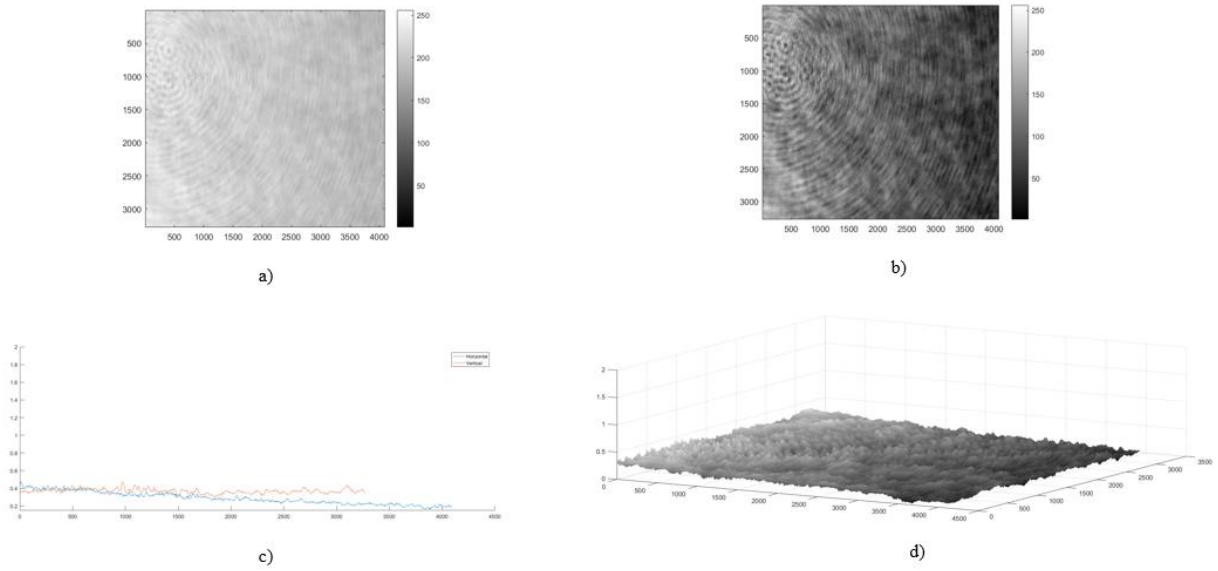

Figure 4.15 Results for 5 nanorad tilt introduced into the system using four-step phase shifting method, a) raw image of the interference pattern, b) Phase map, c)2D unwrapped phase plot and d)3D unwrapped phase plot.

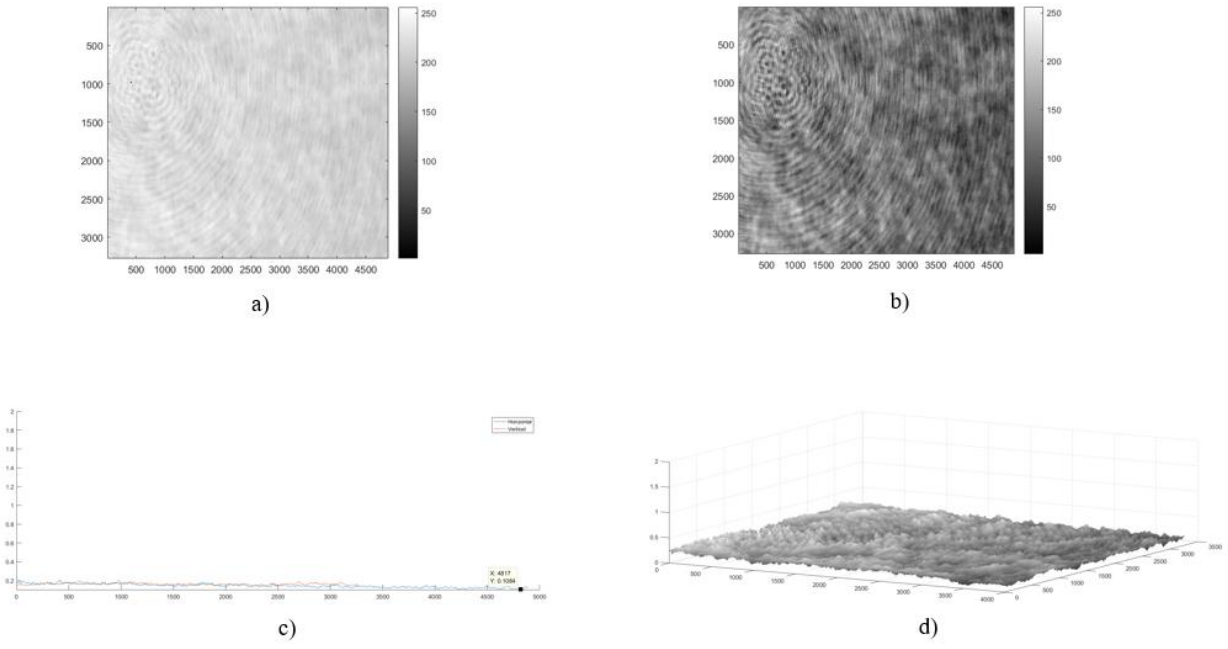

Figure 4.16 Results for 2 nanorad tilt introduced into the system using four-step phase shifting method, a) raw image of the interference pattern, b) Phase map, c)2D unwrapped phase plot and d)3D unwrapped phase plot.

Table 4.1 Introduced tilt vs measured tilt for cyclic interferometer with one reflection using four-step phase shifting method.

Introduced tilt (nrad)	Phase Measured (max-min)	Size of image (pixels)	Measured tilt (nrad)	Experimental Error (nrad)
1000	41.8	3820x4896	4055.8	0.3
500	20.84	3820x4896	2022	0.1
400	16.68	3820x4896	1618.6	0.1
300	12.46	3820x4896	1209	0.1
200	8.36	3820x4896	811.2	0.2
100	4.16	3820x4896	403.6	0.1
50	2.08	3820x4896	201.8	0.1
10	0.42	3820x4896	40.56	0.2
5	0.20	3820x4896	20.2	0.1
2	0.08	3820x4896	8.4	0.1

The results of the measured tilt against the introduced tilt using the four-step phase shifting method shows a very good agreement within experimental error. The maximum phase was measured for each tilt, and the measured tilt was calculated by converting the phase to wavefront distances in wavelength. Then, tilt was determined from the number of pixels and the pixel size of the sensor. Do note that magnification factor does not influence the tilt angles determined by the cyclic interferometer. The graph in Fig. 4.17 shows the results of the measured and the introduced tilt in the cyclic interferometer with one reflection. Also tilt measurement is done as high as 1.00 μrad to 2 nanorad by evaluating phase.

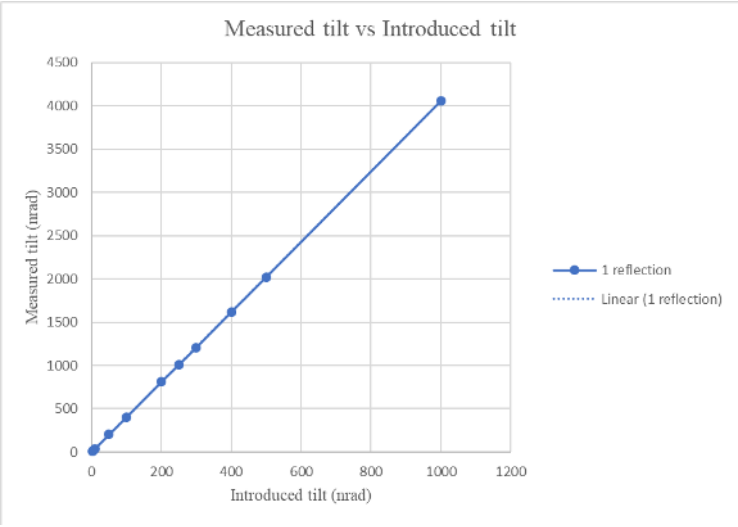

Figure 4.17 Measured tilt (nrad) vs. introduced tilt (nrad) using the four-step phase shifting method.

The average error for these measurements is 0.2 nanorad. Error in these experiments is based on the determination of the phase at every point using the four-phase step method. Errors in the value of the phase step can cause unwanted ripples in the phase map. An additional error in the phase value can be caused by noise in generating the phase maps as well.

4.4 Quantitative measurement using fringe differentiation method

One of the problems that can be faced when using the four-phase step polarization method is that the visibility of the fringes is not constant. This can happen if the axis of the quarter-wave plate is not located 45 degrees with respect to the incident polarization state, This causes the beam exiting the quarter-wave plate to be elliptically polarized. When introducing phase steps by rotating the half-wave plate, the two beams thus will result in different amplitudes. When this happens then the visibility of the fringes when introducing a series of phase step of $\pi/2$ will not be constant. This will create higher order ripples in the phase maps and therefore introduce errors. Therefore, a phase differentiation method was proposed whereby the effect of the change in visibilities is removed in the phase calculation. In this method only two images of the fringes are required where there is a phase step of $\pi/2$ between the two images. Here Δx used in extracting the slope is determined by the number of fringes and usually it is 1/4 of the fringe width. Once this was accomplished, the phase maps and the 3D plot of the tilt were generated by using either equation 3.24 or 3.37. With careful alignment along x, y and z axis, a uniform visibility of the fringes was maintained. Thus Equation 3.24 was used for phase calculations. The following figure shows this result.

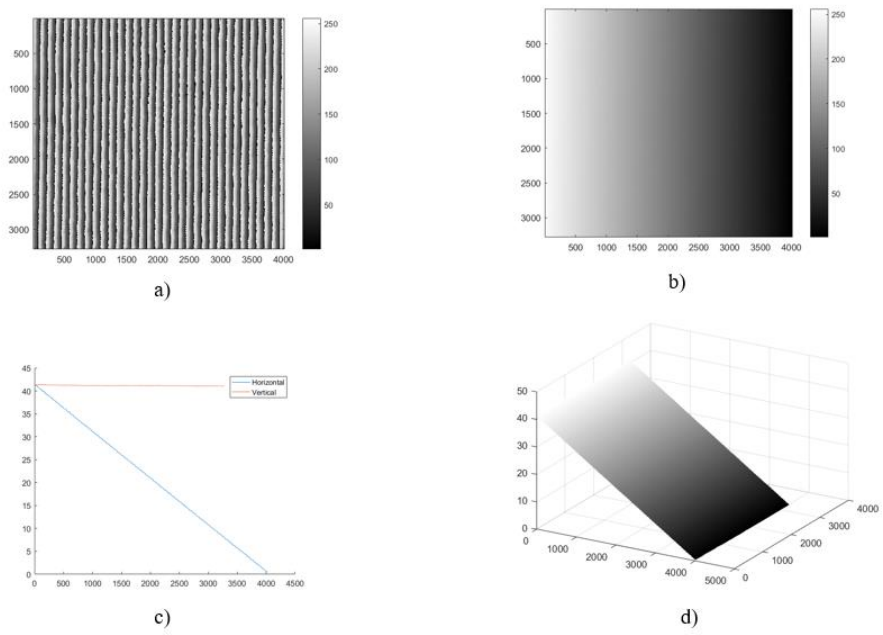

Figure 4.18 Results for 1000 nanorad tilt introduced into the system using phase differentiation method, a) raw image of the interference pattern, b) Phase map, c)2D unwrapped phase plot and d)3D unwrapped phase plot.

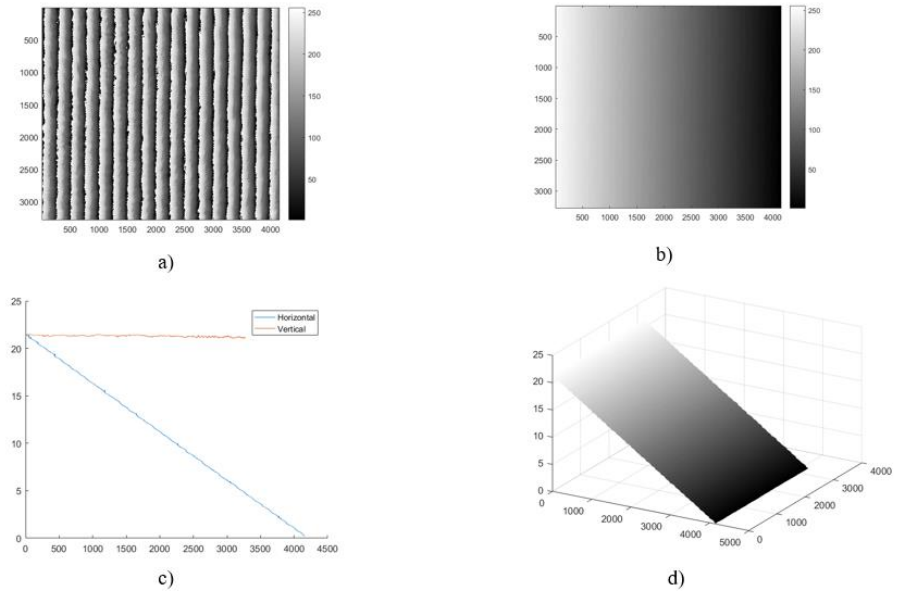

Figure 4.19 Results for 500 nanorad tilt introduced into the system using phase differentiation method, a) raw image of the interference pattern, b) Phase map, c)2D unwrapped phase plot and d)3D unwrapped phase plot.

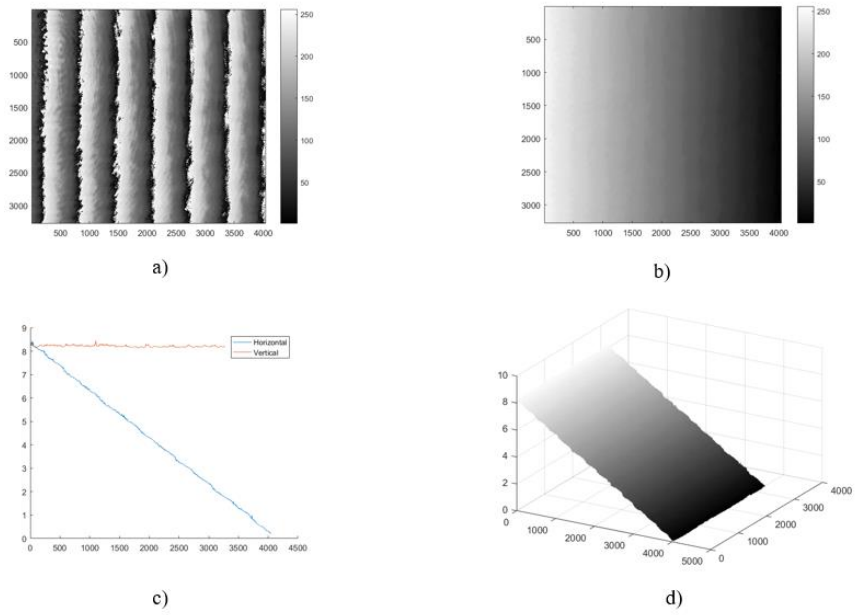

Figure 4.20 Results for 200 nanorad tilt introduced into the system using phase differentiation method, a) raw image of the interference pattern, b) Phase map, c)2D unwrapped phase plot and d)3D unwrapped phase plot.

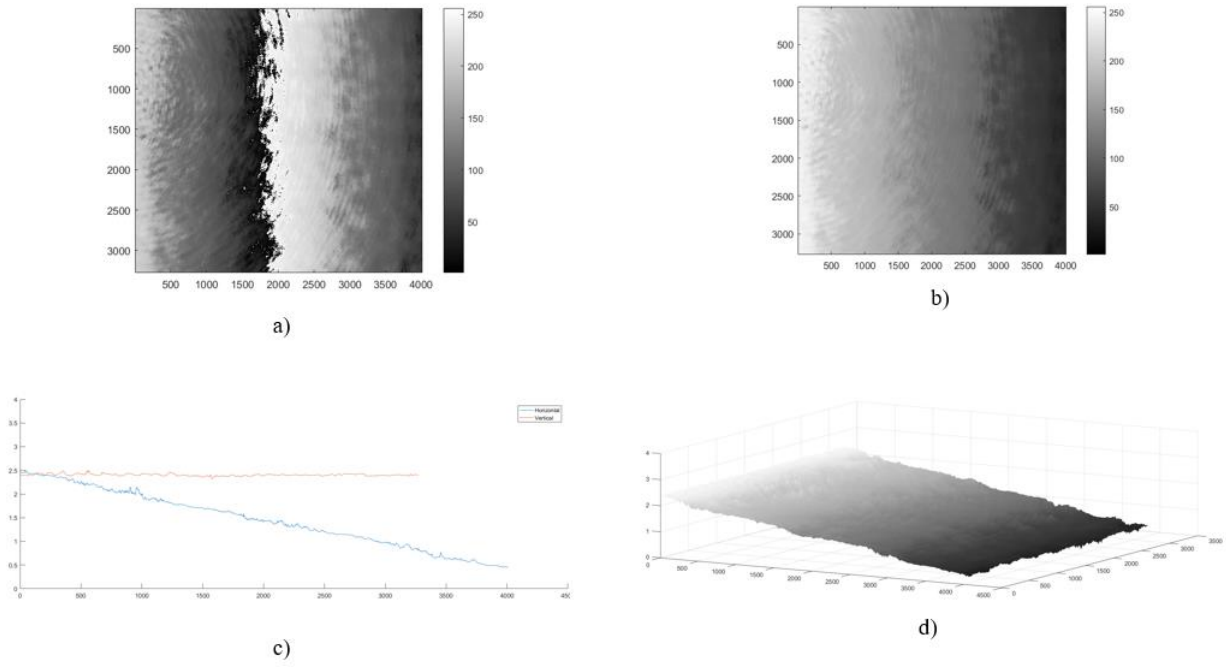

Figure 4.21 Results for 50 nanorad tilt introduced into the system using phase differentiation method, a) raw image of the interference pattern, b) Phase map, c)2D unwrapped phase plot and d)3D unwrapped phase plot.

As shown in Table 4.2, the results of the measured tilt against the introduced tilt using the phase differentiation method shows a very good agreement. The maximum phase was measured for each tilt and then the measured tilt was calculated. The graph in Fig. 4.22 shows that the phase differentiation method has more accurate results.

Table 4.2 Introduced vs measured tilt for cyclic interferometer with one reflection using the phase differentiation method.

Introduced tilt (nrad)	Phase Measured (max-min)	Size of image (pixels)	Measured tilt (nrad)	Experimental Error (nrad)
1000	41.46	3820x4896	4022	0.1
500	20.68	3820x4896	2006.6	0.1
200	8.32	3820x4896	807.2	0.2
50	2.06	3820x4896	200.2	0.1

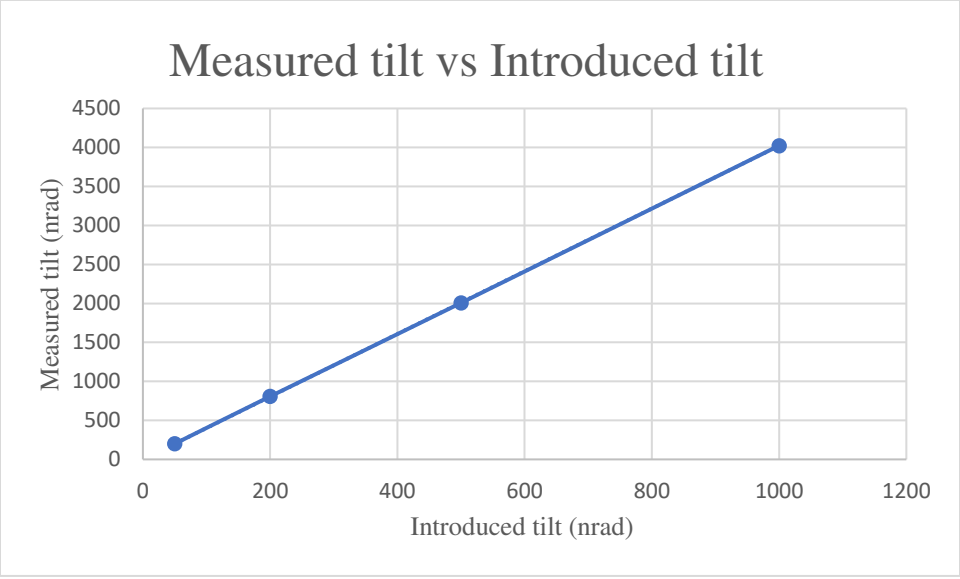

Figure 4.22 Measured tilt (nrad) vs. introduced tilt (nrad) using the phase differentiation method.

4.5 Introducing multiple reflections and measuring the tilt

In order to introduce multiple reflections into the system, a flat square mirror M4 with dimensions of 75*75 mm^2 was introduced, as is shown in Fig 4.2.

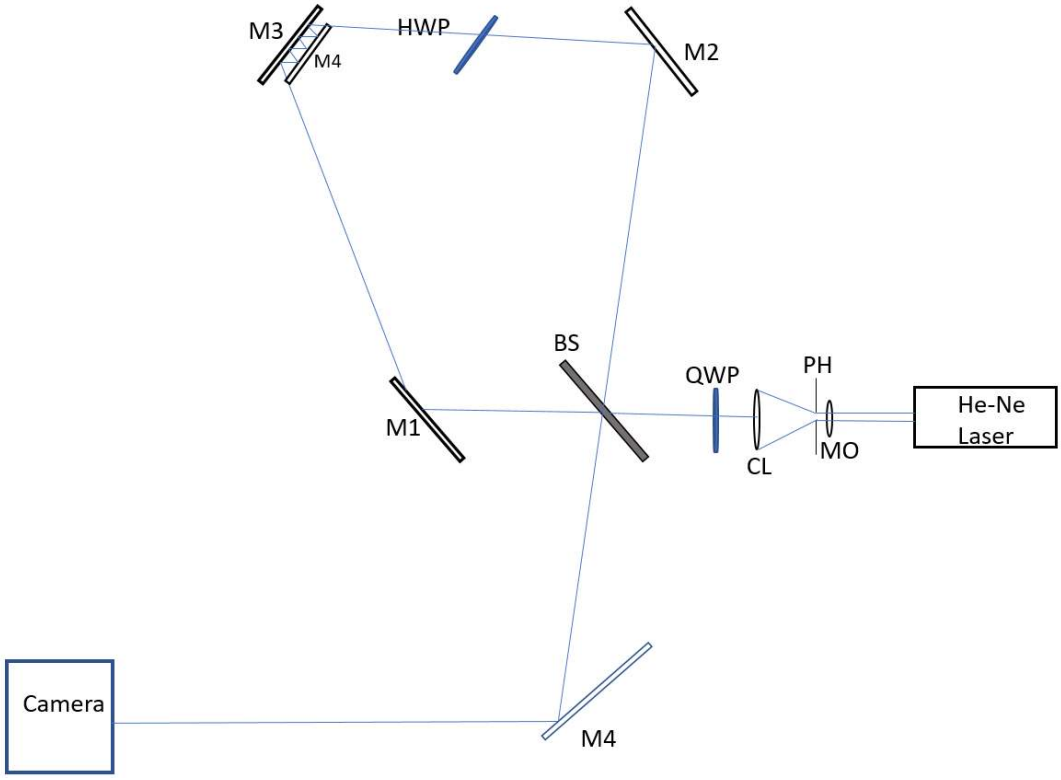

(4.2)

Figure 4.23 Schematic of the cyclic interferometer in order to add multiple reflections (M4 is the tilting mirror).

The distance between M3 and M4 is set at 8 mm while the length of M4 (tilting mirror) is 50 mm. This geometry allows for the incident angle at the interface of mirror M3 to be 38°, and thus four reflections can be accommodated with this two-mirror geometry. The setup was adjusted to make sure that the least amount of diffraction from the edges of the mirrors had occurred. To reduce the size of the laser beam, an iris was placed between the QWP and BS. The results for the 4 reflections introduced on M4 are shown in the following. Table 4.3 gives the introduced tilt vs. the measured tilt using the four-step phase shifting method and multiple reflections.

$$N = \frac{1}{2d} \cdot \frac{L}{\tan(\theta)}$$

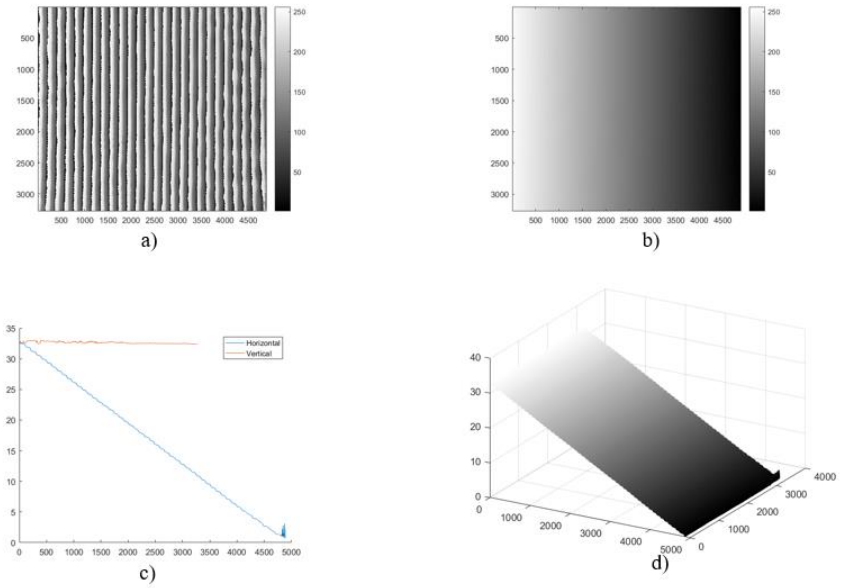

Figure 4.24 Results for 200 nanorad tilt introduced into the system with multiple reflections using four-step phase shifting method, a) raw image of the interference pattern, b) Phase map, c)2D unwrapped phase plot and d)3D unwrapped phase plot.

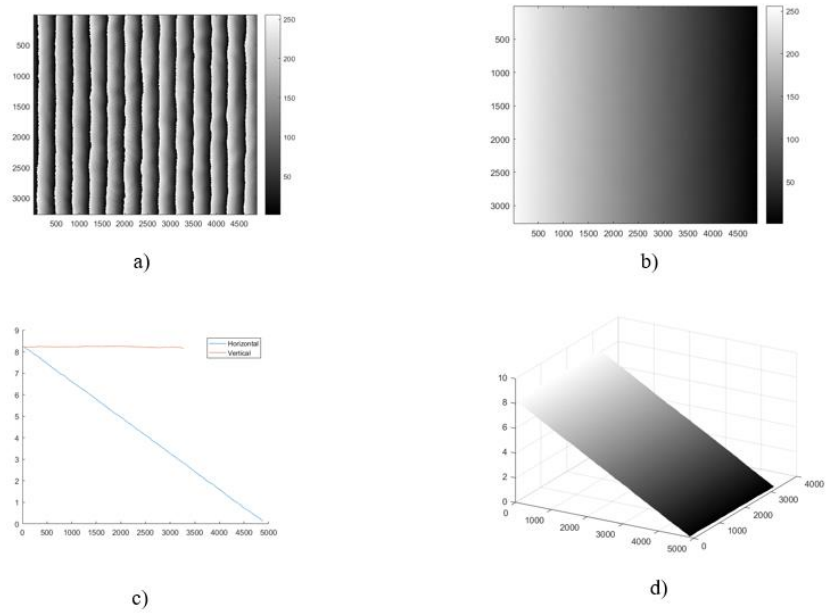

Figure 4.25 Results for 100 nanorad tilt introduced into the system with multiple reflections using four-step phase shifting method, a) raw image of the interference pattern, b) Phase map, c)2D unwrapped phase plot and d)3D unwrapped phase plot.

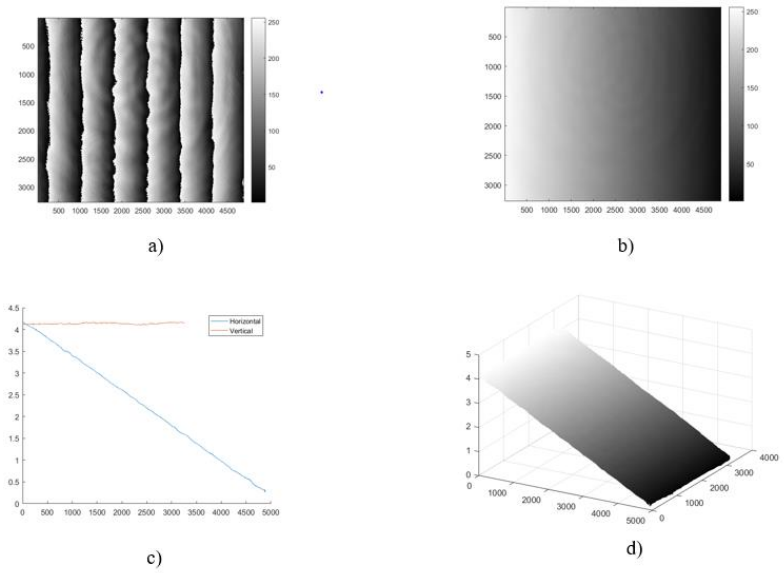

Figure 4.26 Results for 50 nanorad tilt introduced into the system with multiple reflections using four-step phase shifting method, a) raw image of the interference pattern, b) Phase map, c)2D unwrapped phase plot and d)3D unwrapped phase plot.

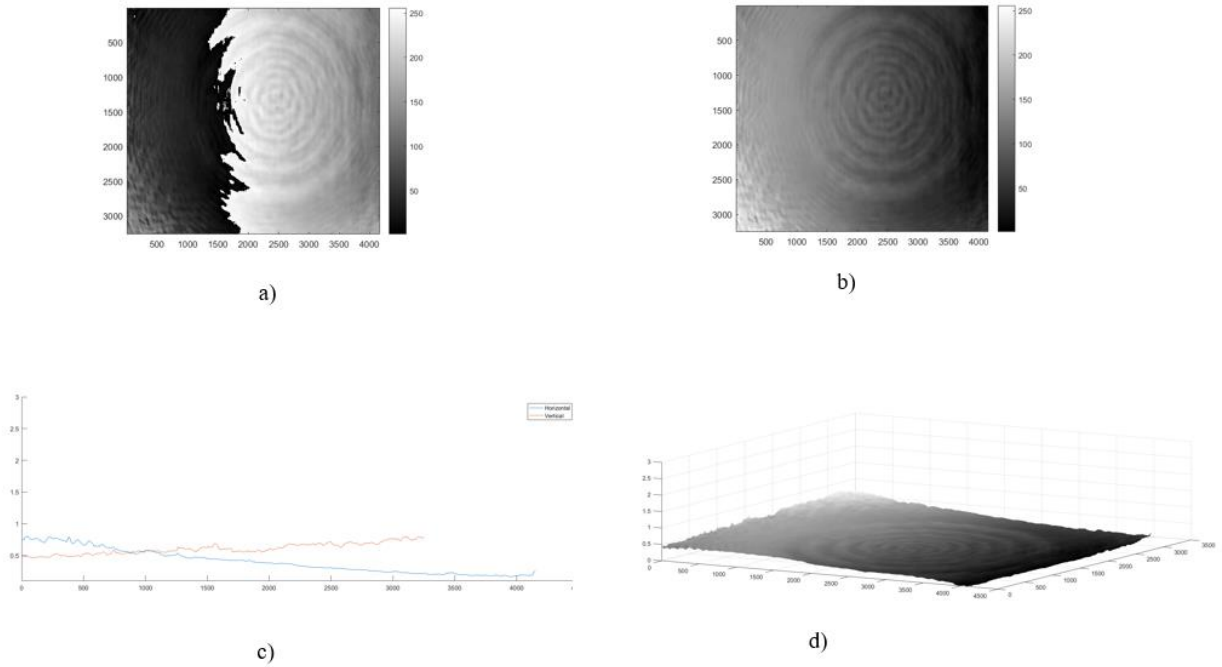

Figure 4.27 Results for 10 nanorad tilt introduced into the system with multiple reflections using four-step phase shifting method, a) raw image of the interference pattern, b) Phase map, c)2D unwrapped phase plot and d)3D unwrapped phase plot.

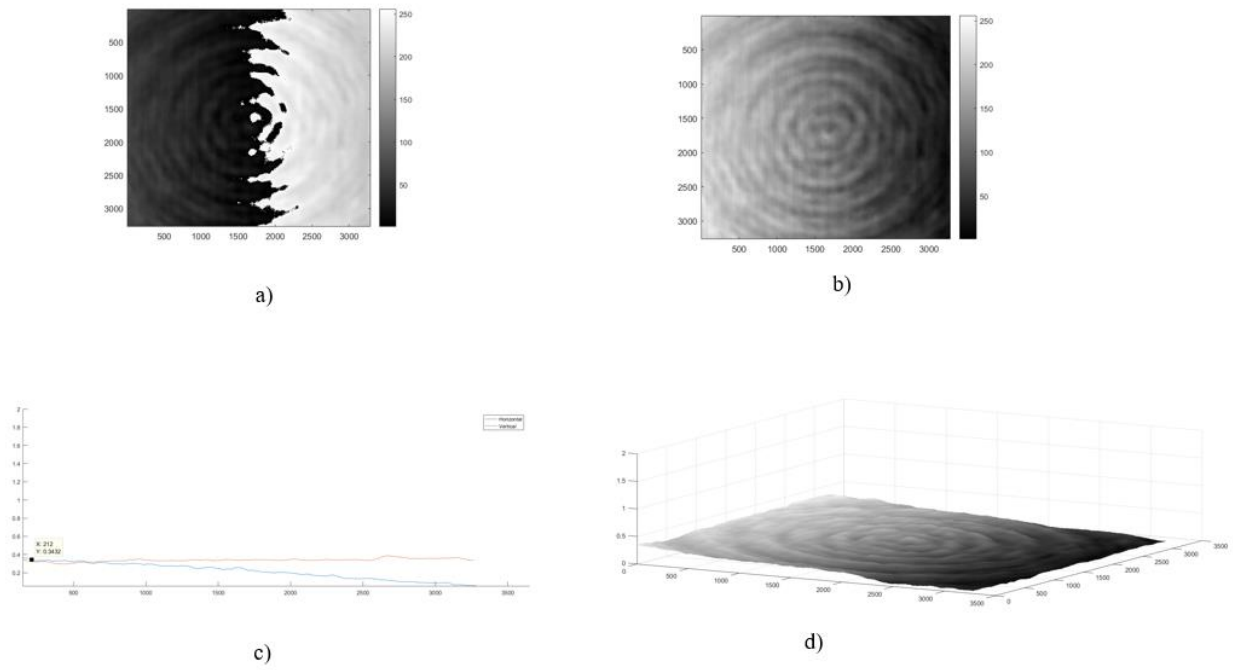

Figure 4.28 Results for 2 nanorad tilt introduced into the system with multiple reflections using four-step phase shifting method, a) raw image of the interference pattern, b) Phase map, c)2D unwrapped phase plot and d)3D unwrapped phase plot.

Table 4.3 Introduced vs. measured tilt achieved with multiple reflection cyclic interferometer using four-step phase shifting method.

Introduced tilt (nrad)	Phase Measured (max-min)	Size of image (pixels)	Measured tilt (nrad)	Experimental Error (nrad)
200	33.01	3820x4896	3204	0.1
100	16.56	3820x4896	1606.8	0.1
50	8.32	3820x4896	807.2	0.1
10	1.62	3820x4896	161	0.1
5	0.868	3820x4896	84.2	0.1
2	0.33	3820x4896	32.2	0.1

As can be seen in Table 4.3 and Fig 4.30, the slope of the graph for the multiple reflections is multiplied by 4, since there were 4 reflections on the tilting mirror, which agrees with the theory explained in chapter 3.

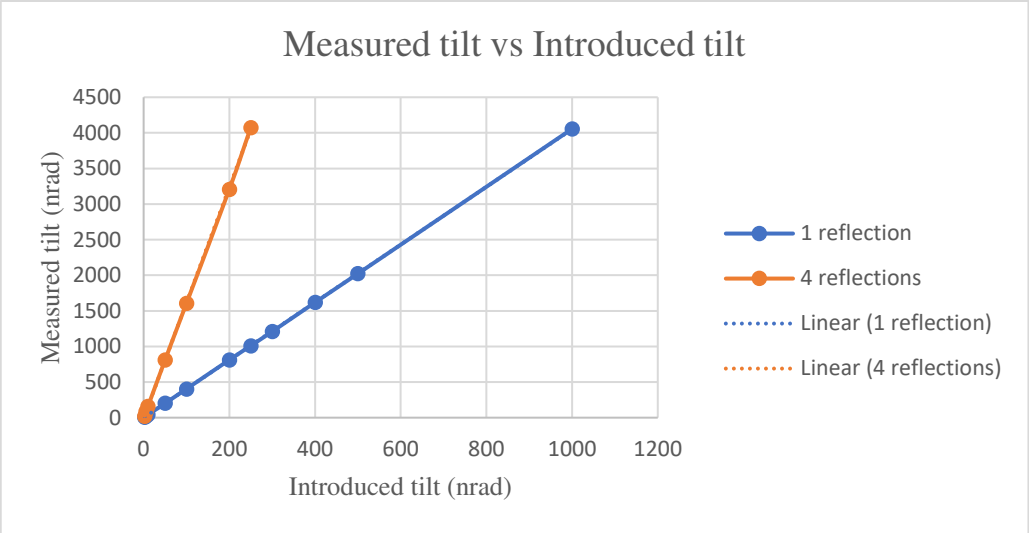

Figure 4.30 Measured tilt vs introduced tilt comparison for 1 and 4 reflections using four-step phase shifting method.

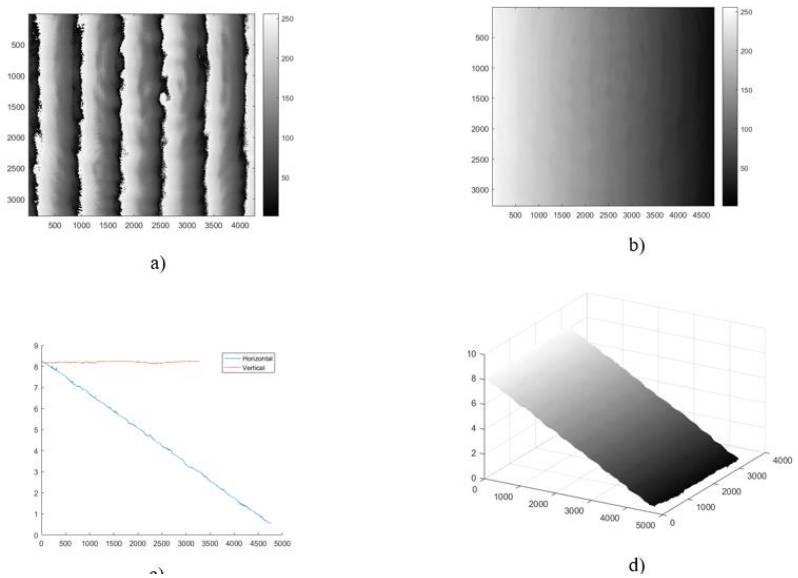

Figure 4.29 Results for 50 nanorad tilt introduced into the system using phase differentiation method with multiple reflections, a) raw image of the interference pattern, b) Phase map, c)2D unwrapped phase plot and d)3D unwrapped phase plot

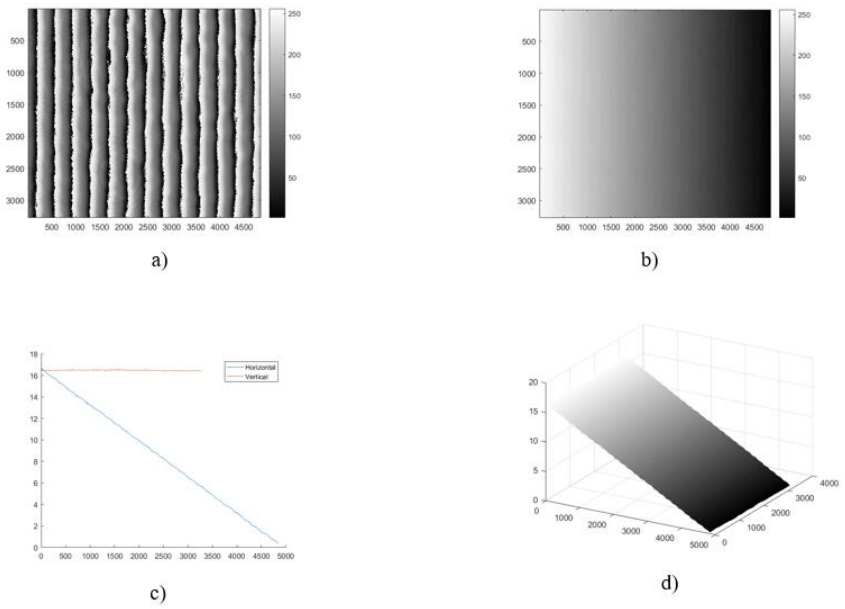

Figure 4.31 Results for 100 nanorad tilt introduced into the system using phase differentiation method with multiple reflections, a) raw image of the interference pattern, b) Phase map, c)2D unwrapped phase plot and d)3D unwrapped phase plot.

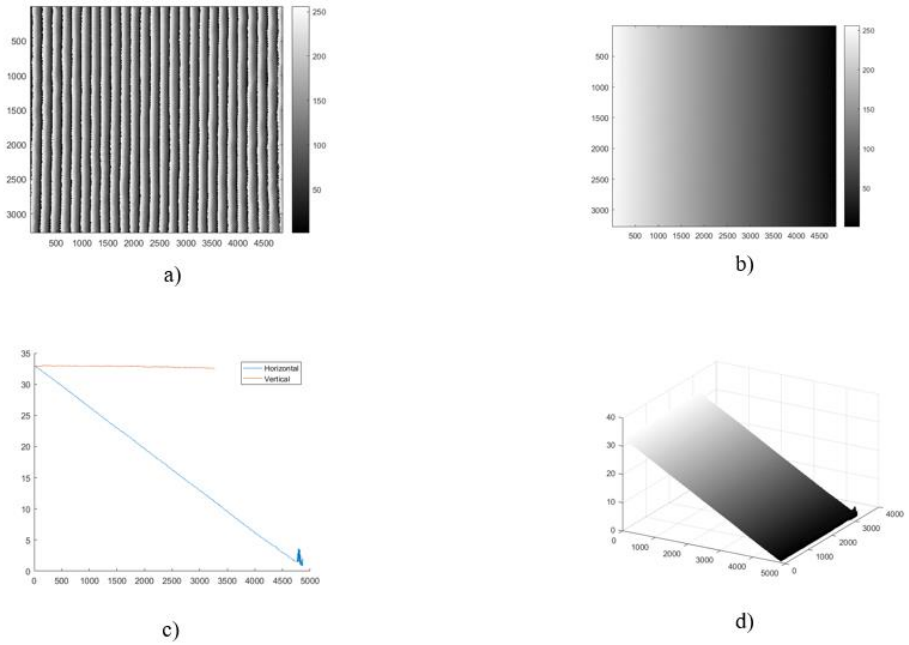

Figure 4.32 Results for 200 nanorad tilt introduced into the system using phase differentiation method with multiple reflections, a) raw image of the interference pattern, b) Phase map, c)2D unwrapped phase plot and d)3D unwrapped phase plot.

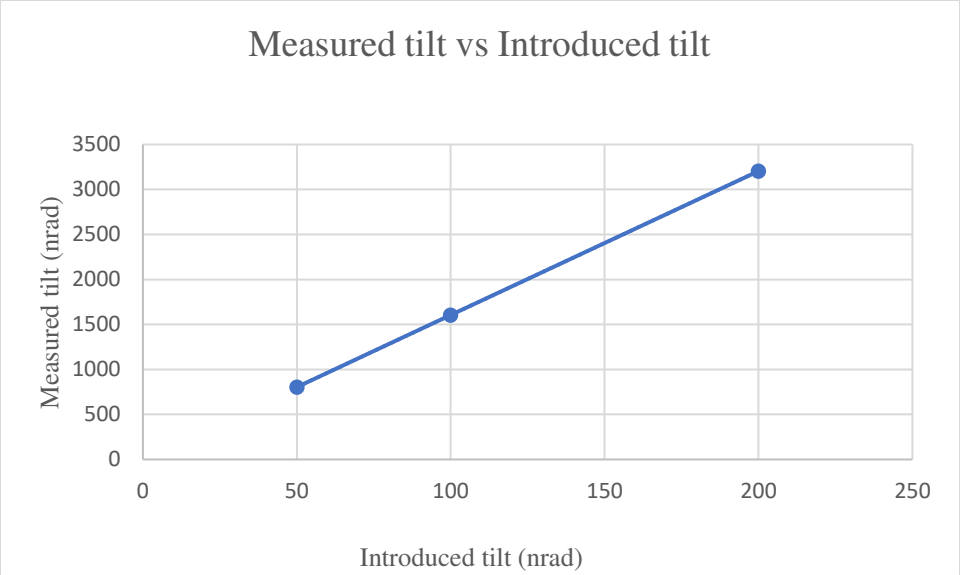

Figure 4.33 Measured vs. introduced tilt using phase differentiation method with multiple reflections.

Table 4 shows the measured vs. the calculated tilt using the phase differentiation method, as shown in the results for the system without multiple reflections, this method is more accurate according to the slope of the fitted lines to the data points, Fig. 4.30 and Fig. 4.34.

Table 4.4 Introduced vs measured tilt in multiple reflection cyclic interferometer using phase differentiation method.

Introduced tilt (nrad)	Phase Measured (max-min)	Size of image (pixels)	Measured tilt (nrad)	Experimental Error (nrad)
200	33.02	3820*4896	3204	0.1
100	16.54	3820*4896	1604.8	0.1
50	8.28	3820*4896	804.4	0.1

5 Conclusion

In this thesis, tilt angles were measured using a cyclic interferometer in the nanoscale region. Tilt angles as small as 2nrads were measured with high accuracy and sensitivity. The error was low, indeed as 0.1 nanoradians.

A novel and simple polarization phase shifting method was developed for this purpose of measuring such small angles. The polarization method uses only one quarter-wave and one half-wave plate unlike other methods proposed in the literature. Using few components allows for less stringent need on the beam quality after passing through each optical component. In evaluating phase using the phase step method, a four-phase step and the phase differentiation method was used. The use of the differentiation method comes handy because it requires only two images to captured unlike the four-phase step method, which requires four images. In the case of changing visibility, a new algorithm was developed to calculate phase using the phase differentiation method. In order to introduce the polarization phase shift, a quarter wave plate was used before the BS to turn the linearly polarized light into a circularly polarized light. In one of the arms of the interferometer, a half-wave plate was used to shift the phase. It is worth mentioning that for the four-step phase shifting method four images were captured within 22.5^{o} steps.

Also, a new method was introduced that is able to evaluate the phase and eventually measure the tilt even in the case of varying visibility. This can be done by using two images which have a $\pi/2$ phase difference. The results for this technique show that the cyclic interferometer can be used to measure object tilts in the nanoscale region.

An additional advantage of the cyclic interferometer is that the two counter propagating beams travel identical paths and thus the interferometer is insensitive to external vibrations and turbulences.

Multiple reflections were introduced in the cyclic interferometer to enhance tilt measurement capability. Using two mirrors that are parallel to each other, the beams were able to go through four multiple reflections before being combined at the BS. Thus, the minimum tilt angle that is measured was reduced by the number of multiple reflections. So, tilt as low as 0.2 nanoradians or 10^{-5} arc of a second was measured. In principle, by increasing the number of reflections this value could be further reduced. It is easy to create about 10 reflections with the size of the mirrors used in this setup. Therefore the lower limit is set at 0.2 nanoradians or 4×10^{-5} arc of a second.

For future work, a tilt stage with higher resolution can be used to introduce tilts in the order of picoradians that can be measured using this system. The effect of different aberrations on this interferometer can also be studied in future work. In addition, the number of reflections can be further increased based on the size of the mirror and the input angle as well.

6 References

[1] A. Bergamin, G. Cavagnero, G. Durando, G. Mana and E. Massa, "A two-axis tip–tilt platform for x-ray interferometry," *Measurement Science and Technology,* p. 717, 2003.

[2] M. A. C. Perryman, "An astrometric and photometric survey of our galaxy," *Astrophysics and Space Science (Springer Science Business media),* 2002.

[3] S. K. Lamoreaux, "Demonstration of the Casimir force in the 0.6 to 6 micrometer range," *Phys. Rev. Lett.,* vol. 78, pp. 5-8, 1997.

[4] R. Wiesendanger, Scanning Probe Microscopy and Spectroscopy:Methods and Applications, UK: Cambridge U. Press, 1994.

[5] T. J. Quinn, C. C. Speake and and R. S. Davis, "Novel torsion balance for the measurement of the Newtonian gravitational constant," *Metrologia,* no. 34, pp. 245-249, 1997.

[6] D. Malacara, Optical Shop Testing, New Jersey: John Wiley and Sons, 2007.

[7] S. Lin, S. Yeh and a. Z. Lin, "Angular Probe based using Fabry-Perot etalon and scanning technique," *Optics Express,* vol. 18, no. 3, pp. 1794-1800, 2011.

[8] O. Harris and D. Malacara, "Interferometric measurements of angles," *Applied Optics,* vol. 9, no. 7, pp. 1630-1633, 1970.

[9] S. Trocpy, L. Chassagne, D. Haddad and Y. Alaylid, "Heterodyne interferometric technique for displacement control at the nanometric scale," *Rev. Sci. Instrum.,* vol. 74, no. 11, pp. 4876-4880, 2003.

[10] V. Kumar, C. Joenathan, A. Ganesan and U. Somasundram, "Increasing the sensitivity for tilt measurement using a cyclic interferometer with multiple reflections," *Optical Engineering,* vol. 55, no. 8, pp. 084103_1-084103_8, 2016.

[11] C. Joenathan, A. Bernal, Y. Woonghee, R. Bunch and C. Hakoda, "Dual-arm multiple-reflection Michleson Interferometer for large multiple reflections and increased sensitivity," *optical Engineeering,* vol. 55, no. 2, pp. 024101-8, 2016.

[12] Britannica, "Encyclopædia Britannica," 21 January 2011. [Online]. Available: https://www.britannica.com/science/interference-fringe. [Accessed 16 April 2017].

[13] P. Hariharan, Basics of Interferometry, Elsevier, 2007.

[14] J. Villate, "fisica.fe.up.pt," Faculty of Engineering of the University of Porto, 15 September 2006. [Online]. Available: http://fisica.fe.up.pt/michelson. [Accessed 16 April 2017].

[15] M. Chiu, C. Chen and D. Su, "Method for measuring the fast axis and phase retardation of a wave plate," *Optical Engineering,* vol. 36, no. 6, pp. 1750-1753, 1996.

[16] M. Su and D. Chu, "Angle mesaurement using total internal reflection heterodyne interferometry," *Otical Engineering,* vol. 36, no. 6, pp. 1750-1753, 1997.

[17] A. A. Michelson, Light waves and their use, Chicago: Chicago Univercity Press, 1903.

[18] P. Hariharan, "Sagnac or Michelson-Sagnac interferometer?," *Applied Optics,* vol. 14, pp. 2319-2321, 1975.

[19] O. D. Soares, "Analysis and alignment of cyclic interferometer," *Journal of Phys. E: Sci. Instrum.,* vol. 11, pp. 773-776, 1978.

[20] Y. P. Kumar, S. Chatterjee and S. S. Negi, "small roll angle measurement using latteral shearing cyclic path polarization interferometry," *Applied Optics,* vol. 55, pp. 979-983, 2016.

[21] F. Fargo and M. Curtis, From Handbook of Dimensional Measurement,, New York: Industrial Press, 1994.

[22] M. Pisani and M. Astrua, " "Angle Amplification for nanoradian measurements," *Applied Optics,* vol. 45, no. 8, pp. 1725-1729, 2006.

[23] V. P. Kumar, A. Ganesan, C. Joenathan and U. Somasundaram, "Effect of beam quality on tilt measurement using cyclic interferometer," in *Interferometry XVIII-SPIE*, 2016.

[24] J. Novak, "Computer Analysis of Interference Fields Using MATLAB," *Dept. Of Pysics CTU Prague.*

[25] J. Wyant, "University of Arizona College of Optical Sciences," 2016. [Online]. Available: https://wp.optics.arizona.edu/jcwyant/wp-content/uploads/sites/13/2016/08/Introduction_to_Interferometric_Optical_Testing.pdf. [Accessed 12 May 2017].

[26] C. Joenathan, "Phase measuring interferometry: new methods and error analysis," *Applied Optics,* vol. 33, pp. 4147-4155, 1994.

[27] C. Joenathan and B. Khorana, "Phase measurement by differentiating interferometric fringes," *Modern Optics,* vol. 39, no. 10, pp. 2075-2087, 1992.